Dissertation presented to the Instituto Tecnológico de Aeronáutica, in partial fulfillment of the requirements for the degree of Master of Science in the Graduate Program of Aeronautical and Mechanical Engineering, Field of Aeronautical Design, Aerospace Systems and Structures.

Danilo Moura Prata

A SEMI-ANALYTICAL MODEL FOR THERMO-MECHANICAL STRESS ANALYSIS IN COMPOSITE LAMINATES

Dissertation approved in its final version by signatories below:

Maurício Vicente Donadon

Prof. Dr. Maurício Vicente Donadon
Advisor

Campo Montenegro
São José dos Campos, SP – Brazil
2024

Cataloging-in Publication Data
Documentation and Information Division

Moura Prata, Danilo
A Semi-Analytical Model for Thermo-Mechanical Stress Analysis in Composite Laminates / Danilo Moura Prata
São José dos Campos, 2024.
75f.

Dissertation of Master of Science – Course of Aeronautical and Mechanical Engineering. Area of Aeronautical Design, Aerospace Systems and Structures – Instituto Tecnológico de Aeronáutica, 2024. Advisor: Prof. Dr. Maurício Vicente Donadon

1. Materiais compósitos 2. Deformação. 3. Método de Rayleigh-Ritz. 4. Laminados. 5. Tensão residual 6. Engenharia de materiais I. Instituto Tecnológico de Aeronáutica. II. A Semi-Analytical Model for Thermo-Mechanical Stress Analysis in Composite Laminates.

BIBLIOGRAPHY REFERENCE

MOURA PRATA, Danilo. **A Semi-Analytical Model for Thermo-Mechanical Stress Analysis in Composite Laminates**. 2024. 75 f. Dissertation of Master of Science – Instituto Tecnológico de Aeronáutica, São José dos Campos, 2024.

CESSION OF RIGHTS

AUTHOR´S NAME: Danilo Moura Prata
PUBLICATION TITLE: A Semi-Analytical Model for Thermo-Mechanical Stress Analysis in Composite Laminates.
PUBLICATION KIND/YEAR: Dissertation / 2024

_____

Danilo Moura Prata
Vila Sônia, São Paulo
CEP: 05.633-010, São Paulo - SP

A SEMI-ANALYTICAL MODEL FOR THERMO-MECHANICAL STRESS ANALYSIS IN COMPOSITE LAMINATES

Danilo Moura Prata

Thesis Committee composition:

Prof. Dr.	Airton Nabarrete	President	-	ITA
Prof. Dr.	Maurício Vicente Donadon	Advisor	-	ITA
Prof. Dr.	Sérgio Gustavo Ferreira Cordeiro	Internal Member	-	ITA
Prof. Dr.	Gerson Marinucci	External Member	-	IPEN

ITA

I dedicate this work to my family and friends who, throughout this period, provided unwavering support and commitment, guiding me like a sturdy boat through stormy seas. Their presence and dedication were my compass, helping me navigate the turbulent waters of life's journey and moor with a deeper understanding for the life beauty that surrounds us.

Acknowledgments

I would like to express my gratitude to the Diretoria de Desenvolvimento Nuclear da Marinha (DDNM) for providing me with the opportunity to launch my career, enabling me to soar at the Instituo Tecnológico de Aeronáutica.

I am also thankful to Professor Maurício Vicente Donadon for his teachings and trust, which guided me through every stage of this work, even when I doubted my own abilities.

My heartfelt thanks go to all ITA professors who wisely taught the subjects I studied and contributed to the skills necessary for this work. I am grateful to my laboratory colleagues, Geraldo Mauricio Cândido, Hudson Pinheiro Lopes da Silva, and Filipe Caldatto Dalan, for their enthusiastic conversations and camaraderie on all occasions.

Additionally, I would like to thank my classmates, who shared their challenges during the courses, inspiring me to seek solutions to problems.

To my family and friends who admired the challenges of studying at ITA and who continually and fraternally inquired about my progress.

To my wife, Poliana, who believed in my dedication and consistently encouraged me during challenging times.

To my son, Mateus, whose smile, and energy brought moments of joy and allowed me to forget the pressures of time.

"Nunca se haverá de perder o chão ou de colidir contra os fatos se for mantido em vista o caminho percorrido."

(Ernst Mach)

Resumo

Os materiais compósitos constituídos de fibra de carbono de alto módulo e resina termo-fixa têm sido empregados em estruturas avançadas de engenharia, nos mais diversos setores, tais como exploração de petróleo, aeroespacial, energia eólica, dentre outros. Contudo, na fabricação destes materiais, durante o processo de cura responsável pela perfeita adesão entre os constituintes fibra mais matriz, ocorre o surgimento indesejado de pequenas deformações. Tais deformações resultam em tensões residuais, as quais provocam distorções geométricas na peça final, ou diminuem a resistência do material, característica essa tão buscada pelos projetistas ao se adotar os materiais compósitos. Essas tensões residuais são provenientes de efeitos de diferentes naturezas, como térmicos, químicos e até higroscópicos, que ocorrem nos constituintes do compósito devido aos gradientes térmicos e aos fenômenos do comportamento dos materiais sob condições de humidade e pressão, interação da peça com o molde e características de cada processo de fabricação. O cômputo destas tensões pode ser encontrado na literatura aberta, porém, diversos autores, têm desenvolvido metodologias adaptadas especificamente para calcular e prever essas deformações e tensões. O presente trabalho buscou desenvolver e implementar uma ferramenta computacional eficaz na simulação dos efeitos das deformações e tensões residuais de natureza térmica. A abordagem do problema utiliza do Princípio da Estacionariedade da Energia Potencial Total do sistema, permitindo tratar sistemas lineares ou não, considerando a energia interna de deformação e o potencial das forças aplicadas sobre o sistema. A busca da solução do equilíbrio deste sistema é feita através da minimização, via princípios variacionais do potencial total, utilizando o método de aproximação de Rayleigh-Ritz para a determinação dos coeficientes generalizados das séries de funções das equações de equilíbrio, valendo-se das funções de Bardell para descrever as relações deformação-deslocamento. A validação da metodologia é demonstrada pela comparação com casos em que existe solução fechada para os problemas de carregamento mecânico, solução exata para um problema de carregamento térmico, e com simulação via elementos finitos através do software comercial ABAQUS®, evidenciando a efetividade da abordagem adotada.

Abstract

Composite materials made up of high modulus carbon fiber and thermoset resin have been used in advanced engineering structures across a range of sectors, such as oil exploration, aerospace, wind energy, among others. However, undesired small deformations occurs during the manufacturing of these materials, in the curing process responsible for perfect adhesion between the fiber and matrix constituents. These deformations result in residual stresses that can lead to geometric distortions in the final part or reduce the material's strength, a characteristic highly valued by designers when adopting composite materials. These residuals stresses originate from effects of different natures, such as thermal, chemical and even hygroscopic, which occur in the composite constituents due to thermal gradients and material characteristics under the conditions of humidity and pressure, interaction of the part with the mold, characteristics of each manufacturing process. The analysis and calculation of these stresses can be found in specialized literature; however, several authors, have developed adapted methodologies to calculate and predict deformations and stresses. The purpose of this study was to develop and implement a computational tool to simulate the effects of thermal residual deformations and stresses. The adopted approach is based on the Principle of Stationary of the Total Potential Energy of the system, allowing the analysis of linear or non-linear systems, considering the internal deformation energy and the potential of the forces applied to the system. The solution to the equilibrium of the system is to minimize the total potential energy, using the Rayleigh-Ritz approximation method to determine the generalized coefficients of the series of functions in the equilibrium equations, using Bardell functions to describe strain-displacement relations. The validation of the methodology is demonstrated through comparison with cases where closed solutions exist for mechanical loading problems, the exact solution for a thermal loading problem, and finite element simulations using the ABAQUS® commercial software, demonstrating the effectiveness of the adopted approach.

List of Figures

FIGURE 2.1 – A fictitious cure cycle example, showing cure degree, glass transition temperature and resin viscosity development as a function of temperature and time (Adapted from (NIELSEN, 2013)). 22

FIGURE 2.2 – (a) Longitudinal, Transverse and Shear Modulus changes and (b) Poisson´s coefficient changes, observed for the Carbon/Epoxy laminate during cure process – Source Author. 25

FIGURE 2.3 – Longitudinal and Transverse (a) Coefficient of Thermal Expansion (CTE) and (b) Chemical Shrinkage changes, observed of Carbon/Epoxy laminae over time during the cure process – Source Author. 25

FIGURE 2.4 – Tool-part interaction effect in a VARTM process (a) Laminate stretched counter stiffer toll, (b) Interply-Slippage and (c) warpage resulting from demolding (Adapted from (NIELSEN, 2013)). 27

FIGURE 2.5 – Concentric cylinder assemblage of fiber-matrix pairs for a micromechanics-based model (Adapted from (CHEN; ZHANG, 2018)). 28

FIGURE 2.6 – Schematic of a composite part under sliding friction conditions due to tool expansion (Adapted from (YUAN *et al.,* 2016)). 30

FIGURE 3.1 – Warpage of $[20_2/-20_2]$ carbon/epoxy laminate (AS4/3501-6) (Adapted from (DANIEL; ISHAI, 2006)). 34

FIGURE 3.2 – A representative of a Stacking Sequence of laminas resulting in a laminate (Adapted from (DANIEL; ISHAI, 2006)). 36

FIGURE 3.3 – A laminate with generalized forces and moments acting on its midplane, as a result of the layer stresses and strains variation through laminate thickness (Adapted from (DANIEL; ISHAI, 2006)). 37

FIGURE 3.4 – Kinematics of thin lamina (Adapted from (REDDY, 2004)). 38

FIGURE 3.5 – An example of rectangular plate element with natural coordinates (Adapted from (BARDELL, 1991)). 44

FIGURE 3.6 – The first four polynomials of Bardell´s Functions in natural coordinates, (Source Author). 45

FIGURE 3.7 – The first derivative of the first four polynomials of Bardell´s Functions, in natural coordinates, (Source Author). 46

FIGURE 3.8 – An illustration of plate with (a) mid-plane generalized forces and moments (b) transverse load per unit of area, (c) load per unit of length, and (d) transverse concentrated force (Adapted from (REDDY, 2004)). 48

FIGURE 4.1 – An example of cantilever beam loaded at the tip, along with the equation from closed-form solution to compute the maximum deflection (Adapted from (REDDY, 2004)). 52

FIGURE 4.2 – The cantilever beam simulated using the proposed semi-analytical model. 53

FIGURE 4.3 – A cantilever beam with distributed load and the expression for maximum deflection (Adapted from (REDDY, 2004)). 54

FIGURE 4.4 – The cantilever beam simulated using the proposed semi-analytical model. 54

FIGURE 4.5 – An example of biclamped beam with a mid-span mechanical load (Adapted from (REDDY, 2004)). 55

FIGURE 4.6 – The biclamped beam simulated using the proposed semi-analytical model. 55

FIGURE 4.7 – Comparison of deflection along beam length, calculated from the proposed model and literature closed-solution for the clamped beam loaded at the tip. 56

FIGURE 4.8 – Comparison of deflection along beam length, calculated from the proposed model and literature closed-solution for the clamped beam with distributed load. 57

FIGURE 4.9 – An illustration of (a) bi-material beam experimental setup available in (THERMAL, 2022), (c) simulating a clamped bi-material plate-like beam laminate (bonded together) and (b) resulting internal stresses generating a uniform curvature when undergoes a temperature change ΔT. 58

FIGURE 4.10 – The cantilever plate-like beam simulated using the present model. 60

FIGURE 4.11 – The warpage results using (a) CLT model for a non-symmetric $[90_2/0_2]$ composite free plate under thermal load and (b) through the proposed semi-analytical model. 62

FIGURE 4.12 – Warpage result through simulation using the proposed semi-analytical model for a bi-material composite free plate $[90_2/0_2/Al]$ under thermal load. 63

FIGURE 4.13 – Warpage result for the orthotropic laminate plate [45/90/-75/-45] clamped at one edge in y direction using (a) proposed semi-analytical model and (b) FEM ABAQUS®. 65

List of Tables

TABLE 2.1 – Driving mechanisms and its main residual stress effects. 23

TABLE 4.1 – Engineering properties of laminae for E-Glass/Epoxy, from (JONES, 1999). . 52

TABLE 4.2 – Results for the symmetric composite beam simulated. 56

TABLE 4.3 – Engineering properties of Toray Cetex® TC1225 High Strength T300JB 3K Carbon and aluminum layer of Al2024-T4..... 59

Table 4.4 – Results for cantilever bi-material plate-like beam laminate with thermal load only. 60

TABLE 4.5 – Engineering properties of laminae constituents for (AS4/3501-6) (Adapted from (DANIEL; ISHAI, 2006)). 61

TABLE 4.6 – Stresses distributed in each layer for $[90_2 /0_2]$. 62

TABLE 4.7 – Engineering properties of laminae constituents for (Hexcel IM7/913 UD prepreg). 64

TABLE 4.8 – Comparison between results obtained from FEM and from the proposed Semi-Analytical model. 65

List of Abbreviations and Acronyms

ABAQUS	Computation software of FEM Dassault Systèms®
CLT	Classical Lamination Theory
CTE	Coefficient of Thermal Expansion
FEM	Finite Element Method
ITA	Instituto Tecnológico de Aeronáutica
LSDR	Linear Strains-Displacements Relations
MATLAB	Computation software of MathWorks®
PSTPE	Principle of Stationary of the Total Potential Energy
VARTM	Vacuum Assisted Resin Transfer Molding

List of Symbols

α_1	Longitudinal coefficients of thermal expansion
α_2	Transversal coefficients of thermal expansion
a	Laminate length dimension at x-direction
A_{ij}	Extensional stiffness matrix element
β	Chemical Shrinkage Coefficient
b	Laminate width dimension at y-direction
B_{ij}	Bending Extensional coupling stiffness matrix element
δ	Deflection of beam
D_{ij}	Shear-Twist coupling stiffness matrix element
ΔT	Temperature variation
ε	Longitudinal strain
E	Elasticity Modulus of an isotropic material
E_1	Longitudinal Elastic Modulus
E_2	Transversal Elastic Modulus
F_0	Concentrated mechanical load
f_r	Hierarchical polynomial Bardell Function
G_{12}	Shear modulus
η	Non-dimensional coordinate in the y-direction
θ	Angle between one direction in local and global system of coordinates
I	Inertia Moment of Area
κ	Curvature of a thin plate or laminae
υ_{12}	Major Poisson´s ratio
υ_{21}	Minor Poisson´s ratio
ξ	Non-dimensional coordinate in the x-direction
γ_{xy}	Shear in plane strain
λ	Resin structure-dependent parameter
M_x	Generalized moment per unit of length at x-direction
N_x	Generalized forces per unit of length at x-direction
Π	Functional of the total potential energy of a system

q_{ij}	Generalized coordinate
q_0	Distributed mechanical load
T	Temperature
T_g	Glass transition temperature
T_{room}	Room temperature
T_{cure}	Temperature of cure
T_{g_∞}	Glass transition temperature of the fully reacted resin
T_{g_0}	Glass transition temperature of the uncured resin
τ_{12}	Shear stress
t	Laminate thickness
U	Internal strain energy
u_0	Displacement coordinate at x-direction
V_E	Work done by external forces
V_m	Volume Fraction of composite constituent
v_0	Displacement coordinate at y-direction
ϕ	Polynomial function in x-direction
ψ	Polynomial function in y-direction
w_0	Displacement coordinate at z-direction
U	Strain internal energy
χ	Degree of cure of resin

Contents

1 INTRODUCTION 18
1.1 Motivation 18
1.2 Objectives 19
1.3 Dissertation Layout 19
2 LITERATURE REVIEW 21
2.1 Driving Mechanisms for Shape Distortions 21
2.1.1 Intralaminar Stresses from Micromechanics Influence 24
2.1.2 Interlaminar Stresses - A Macroscale Point of View 26
2.1.3 Tool-Part Interaction and Mold Effects 26
2.1.4 Other Factors 27
2.2 Modelling Approaches. 28
2.2.1 Micromechanics-Based Models 28
2.2.2 Interlaminar Analytical Models 29
2.2.3 Variational Based Methods 32
3 SEMI-ANALYTICAL MODEL FORMULATION 33
3.1 Thermal Residual Strains and Stresses 33
3.2 Strain and Stress Variation in a Laminate Thickness 36
3.3 Principle of Stationary of the Total Potential Energy (PSTPE) 41
3.4 Rayleigh-Ritz Approximation Solution 42
3.5 Hierarchical Polynomial Bardell Functions 43
3.6 Proposed Semi-Analytical Model 46
4 RESULTS AND DISCUSSION 51
4.1 Verification of the Proposed Semi-Analytical Model for Mechanical Loading Cases 51
4.1.1 Case 1: Cantilever Composite Plate-Like Beam with a Concentrated Load at the Tip 51
4.1.2 Case 2: Cantilever Composite Plate-Like Beam with Distributed Load 53
4.1.3 Case 3: Bi-Clamped Composite Plate-Like Beam with a Central Load 54
4.2 Verification of the Proposed Semi-Analytical Model for Thermal Loading Cases 57

4.2.1 Case 1: Clamped-Free Bi-Material Plate-Like Beam Laminate Subjected to Thermal Loading 57
4.2.2 Case 2: Monolithic Laminate Plate Subjected to Thermal Loading 61
4.2.3 Case 3: Cantilever Laminate Plate under Thermal Loading 63

5 CONCLUSION 67
5.1 Future Works 68

BIBLIOGRAPHY 70

APPENDIX A – MICROMECHANICS AND GLASS TRANSITION 73
A.1 Engineering Properties of Lamina Changing During Cure 73

1 Introduction

During the manufacturing process of carbon fiber composite, internal stresses may arise from temperature variations in the cure cycle, and the laminate may warp upon tool removal, leading to undesired geometric distortions. These internal stresses induce distortions in laminates and are attributed to many factors such as different cure cycles and the different thermal expansion coefficients of the composite constituents, including fibers, matrix, and metals in hybrid layup schemes. This challenge is frequently encountered in industries such as aerospace, wind turbine, and automotive, which demand complex geometries.

Epoxy resins constitute one of the most critical classes of thermosetting polymers, applied as matrix for fiber-based composites (MAGDALENA, 2011). Temperature effects and conversion to the glassy state significantly influence their performance. Therefore, important mechanisms such as thermal expansion, resin shrinkage, and frozen-in strains developed during curing cycles (MAKINDE, 2018) need to be explored and better understood through analytical methodologies, numerical simulations and/or experimental investigations.

The mechanisms leading to the buildup of residual stresses primarily arise from several factors: the mismatch in thermal-mechanical properties between the fiber and matrix constituents, volume shrinkage of the matrix resulting from the crosslinking process during cure, and the tool-part interaction. The latter occurs when there is a relative motion between the laminate and the mold, as result of the different thermal expansion coefficients between the laminate and the mold (CHEN; ZHANG, 2018).

Consequently, during the manufacturing of fiber-reinforced polymer matrix composites, we often encounter mismatches in geometric dimension between design tolerances and the final part. Such mechanisms should be considered as a complement to the Classical Lamination Theory (CLT), a widely used approach that usually overestimates certain results and overlooks mechanisms, such as micromechanics and the tool-part interaction.

1.1 Motivation

Motivated by the aforementioned issues that may arise during the manufacturing process of thermosetting composites, the present work aimed to analyze, in addition to CLT, the thermal effects after cure process. It addresses a semi-analytical model to simulate the residual strain and stresses in a computation environment, to evaluate the problems encountered after

composite manufacturing process, like warpage in the final part and residual stresses that reduce the strengths of laminate composites (NIELSEN, 2013; WISNOM *et al.,* 2006). The purpose of the investigation is to understand the phenomena involved during the composite curing process and compute the residual strains and stresses to enhance the design step. This understanding allows for the prevention of time and material losses due to geometric distortions and residual stresses in the final part. Furthermore, the research seeks to develop a useful tool for quickly analyzing common problems in structural mechanics. By addressing these issues, the tool can provide significant insights and solutions. This will improve the efficiency and reliability of composite structures.

With this tool, it should be possible to compute the residual strain and stresses in some structural thin parts, like plates, plate-like beams, with a given boundary condition under mechanical and thermal loads or a combination of them. In addition, it is expected that the proposed model can be useful and further extended for other analysis, like panels with curved geometries and cylinders, which can be made by changing the strain-displacement relationships, while maintaining the continuity requirements.

1.2 Objectives

The objectives of this work are:

- To computationally predict residual strains and stresses in thin structural parts, such as plates and plate-like beams to some boundary conditions, under thermal and mechanical loads.
- To evaluate post-fabrication issues, such as warpage and residual thermal stresses.
- To develop a useful computational tool to enhance the design process to prevent geometric distortions and residual stresses in laminates.

1.3 Dissertation Layout

Chapter 2 presents a literature review on the topic, aimed at understanding the main factors involved in residual stresses in thermosetting polymers composite and warpage behavior at flat geometries, as well as briefly explaining the driving mechanisms of the composite constituents.

All the mathematical formulation and key concepts essential for understanding the proposed model are explained in Chapter 3, elucidating their meaning and contribution to the development of this work. The variational method was adopted to obtain the set of equilibrium equations that simulate thermoelastic effects and accounted for the constituent's behavior.

Chapter 4 presents the results obtained using the proposed semi-analytical model for different loading and boundary conditions, comparing the model predictions with closed-form solutions available in the open literature. Moreover, several verification cases are compared to numerical simulations using the software ABAQUS®.

Finally, Chapter 5 draws conclusions and provides future work recommendations.

2 Literature Review

In advanced fiber reinforced composite structures, strategic alignment of high-strength fibers, either in preferred orientations or in hybrid configurations with other materials like metals, yields materials with orthotropic properties (SINKE *et al.*, 2013). Besides, during laminate composite fabrication, internal stresses may arise from temperature variations during the cure cycle, leading to residual strains and stresses and undesired geometric distortions upon tool removal. These challenges are often encountered in industries such as aerospace, wind turbine, and automotive, which demand complex geometries.

The induced distortions in laminates are attributed to factors such as different cure cycles and thermal expansion coefficients of the composite constituents, including fibers, matrix, and metals in hybrid layup schemes. These factors result in residual intralaminar stresses and nonhomogeneous distributions of fibers in the matrix, and residual interlaminar stresses leading to delamination and, sometimes, weak joints between successive plies. Although accurately modelling microscale behaviors of composite materials can sometimes be challenging to assess and require computationally costly analysis, there are other analytical approaches like variational-based methods, which can be easily applied to simulate thermal loads and compute residual stresses at a macroscale, saving computational time and yielding good results. These methods provide accurate predictions of strains and stresses using material parameters, derived from experimental characterization, facilitating the comprehension of such phenomena, and improving residual strains prediction at low computation cost.

2.1 Driving Mechanisms for Shape Distortions

Several studies have investigated the main factors that influence shape distortions due to residual strains and stresses, aiming to enhance the design of composite structures. As an understanding basis, the changing in physical properties of matrix during cure reaction can be mentioned as a main discussion topic.

Lawrence (LAWRENCE, 1969) presented some valuable conclusion about the characteristics of these properties, which may vary due to its dependence on cross-linking effects and glass transition temperature, for thermoset polymers. In his work, it was noted that the cross-linking in polymers significantly affects specific volume and on the thermal

coefficient of expansion, reducing them by decreased mobility of the polymer chains as they become more tightly interconnected. On the other hand, other properties like Elastic Modulus and Creep Resistance increases due to the formation of a more rigid network structure within the polymer. Additionally, the stress-strain properties for rubbers and polymers decreases by reduced chain mobility.

The critical factor for chain-mobility and cross-linking effects is the glass transition temperature (T_g), that is the temperature at which an amorphous polymer changes from a hard, glassy material, to a soft, rubbery state, delimiting when material undergoes significant changes in its mechanical and thermal properties.

Some theoretical models are used to describe the relationship between T_g and cross-link density in thermosetting polymers. A widely used relation to model the curing reaction in thermosetting polymers is the DiBenedetto´s Equation that takes into account the chemical composition and segmental mobility, revealing the shift of the glass transition temperature to degree of cross-linking. This relation allows computing the viscoelastic material behavior and identifying all phase transitions since liquid, passing by rubbery and finally achieving the glassy state of resin during this process of cross-linking formation. Figure 2.1 below shows a schematic of the phase transition during the polymer cure, as the glass transition temperature evolves.

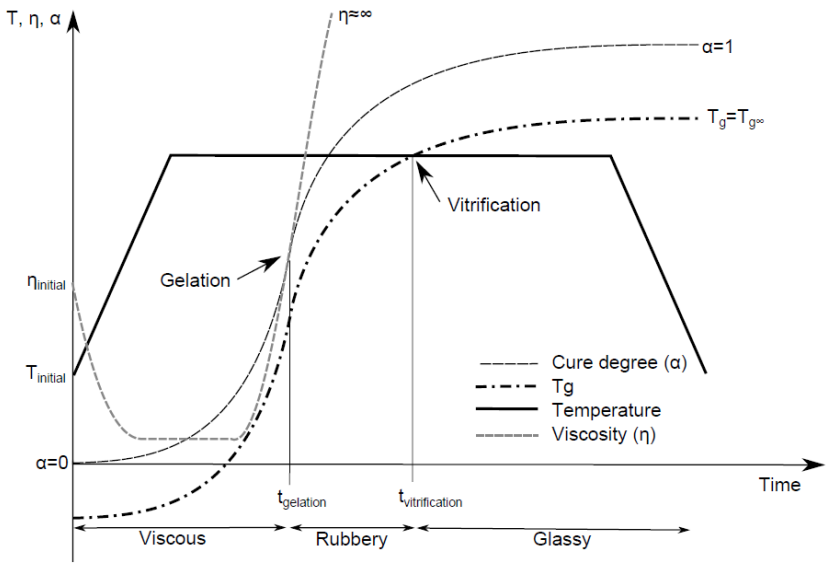

FIGURE 2.1 – A fictitious cure cycle example, showing cure degree, glass transition temperature and resin viscosity development as a function of temperature and time (Adapted from (NIELSEN, 2013)).

To elucidate the main driving mechanisms related to this changing in physical properties and their influence on process-induced distortions in composite structures, several studies can be mentioned. Fernlund (FERNLUND *et al.*, 2003), Wisnom (WISNOM *et al.,* 2006), and Kappel (KAPPEL *et al.*, 2015) have extensively researched and classified these mechanisms, detailing their contributions to stress development during the curing process.

By reviewing open literature, the driving mechanisms can be divided between the intrinsic and extrinsic factors. To understand the extent of influence from these inherent material effects, whether large, medium, or small, one can refer to Nielsen (NIELSEN, 2013) and Makinde (MAKINDE, 2018).

Intrinsic factors can be related to both Intralaminar and Interlaminar stresses. The Intralaminar stresses is based on the micromechanical characteristics as thermal expansion mismatch between fiber and matrix, resin cure shrinkage, void content, and presence of moisture in mixture. Additionally, the Interlaminar stresses emerge from the interaction between successive laminas, which exhibit differences in thermal expansion of each ply as a consequence of the laminate layup.

Furthermore, the Extrinsic factors occur mainly due to external influences, including the cure schedule and difference between Coefficient of Thermal Expansion (CTE) of tool and laminate, which has large contribution to residual stresses and shape distortions in thick laminates.

In summary, Table 2.1 presents the driving mechanisms and their residual stress effects. It is noteworthy to mention that such undesirable issues can often be mitigated by modifying the manufacturing process (CHEN; ZHANG, 2018).

TABLE 2.1 – Driving mechanisms and its main residual stress effects.

Factor	Driving Mechanism	Stress Effect
Intrinsic	Micro-mechanical characteristics	Intralaminar residual stress
	Macromechanical interaction	Interlaminar in-plane stress
Extrinsic	External influences	Tool-Part interaction generating shear stresses

The following sections will provide a more detailed explanation of each specific driving mechanism.

2.1.1 Intralaminar Stresses from Micromechanics Influence

As aforementioned, the Intralaminar stresses within composite materials are significantly influenced by micromechanical interactions between their constituents, particularly noticeable during the curing process.

At the microscale level, residual stresses develop due to several factors, including thermal expansion mismatches between fibers and matrix, in which the Coefficient of Thermal Expansion (CTE) of matrix. Typically, the CTE of the matrix is significantly higher than that of the reinforcement fibers. This leads to fibers and matrix materials expanding and contracting at different rates under temperature changes (NIELSEN, 2013). This discrepancy can induce residual stresses that may compromise the structural integrity of the composite if the material is not properly selected.

Similarly, as the resin cures, linear polymer chains are cross-linked to a denser three-dimensional molecular structure as it transforms from a viscous state to a solid, shrinking in the process and therefore also shrinks composite component (SVANBERG *et al.*, 2005), adding internal stresses through this shrinkage process.

Additionally, voids and moisture within the composite can modify the distribution and magnitude of these stresses, further complicating their prediction and management.

Each one of these factors contributes uniquely to the internal stress profile of a composite, affecting the stress–strain behavior and failures modes, impacting its mechanical performance and reliability under operational conditions. This intricate relationship between micromechanical properties and intralaminar stresses underscores the complexity of predicting and managing residual stresses in composite materials.

Figures 2.2 and 2.3 illustrates the changes of engineering properties, specifically, CTE and Chemical Shrinkage Coefficient over time in the longitudinal and transverse directions for Carbon/Epoxy laminates. These changes, based on its micromechanical behavior, are briefly explained in Appendix A, following the fiber and matrix mixture rule.

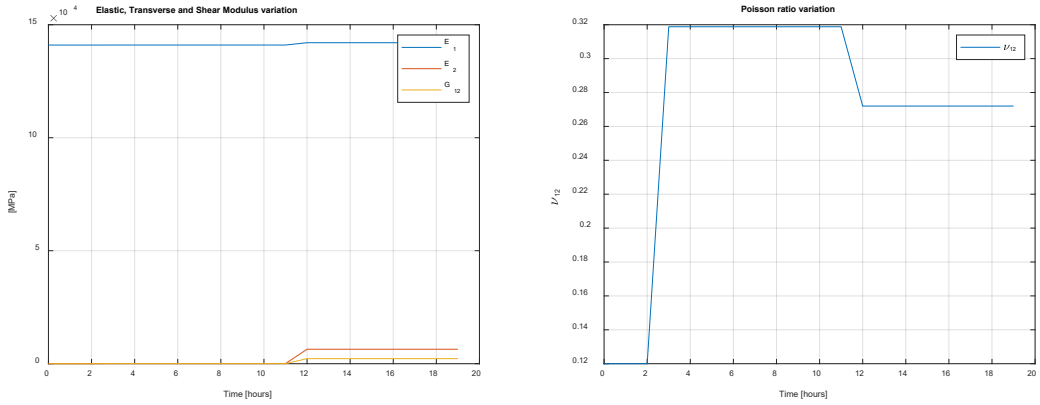

FIGURE 2.2 – (a) Longitudinal, Transverse and Shear Modulus changes and (b) Poisson´s coefficient changes, observed for the Carbon/Epoxy laminate during cure process – Source Author.

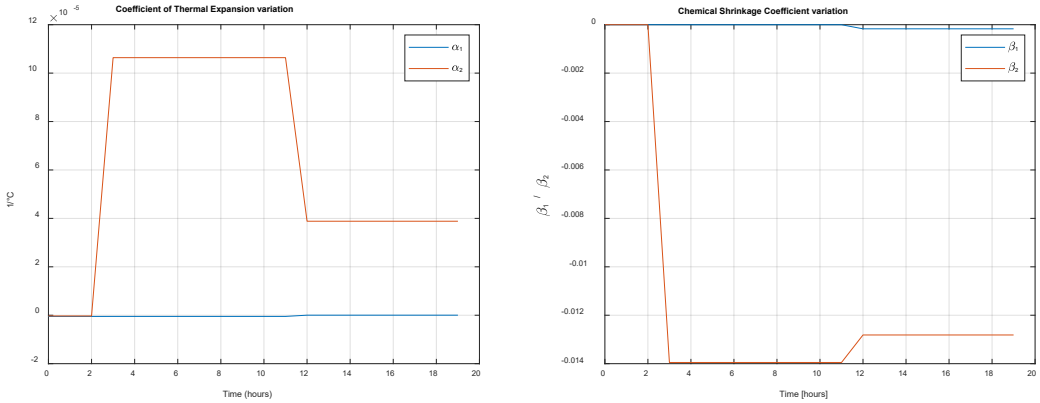

FIGURE 2.3 – Longitudinal and Transverse (a) Coefficient of Thermal Expansion (CTE) and (b) Chemical Shrinkage changes, observed of Carbon/Epoxy laminae over time during the cure process – Source Author.

It is possible to observe the physical properties variation over time during the cure schedule and understand their relation to the stress built-up behavior material, which occurs due to polymer-chain mobility during the three phases illustrated in Figure 1. The equations used to compute those properties can be found in the micromechanics section of Jones (JONES, 1999), employing the fiber and matrix mixture rule, and the input values from Svanberg (SVANBERG; HOLMBERG, 2004b) and Daniel (DANIEL; ISHAI, 2006), resulting in a composite consisting of Carbon Fabric and Araldite LY5052/Hardener HY5052. The steps to compute those properties are described in Appendix A.

2.1.2 Interlaminar Stresses - A Macroscale Point of View

The Interlaminar factors represent another inherent challenge in composite materials, influencing the built-up stresses, which are related to mismatch characteristics in successive plies. Some of these factors have significant influence, such as differences in thermal expansion across laminate layups, and thermal gradients in composite parts for thick laminates. The non-uniform fiber content distribution and gradients in chemical cure within composite can also be a nucleation of residual stresses, but with a moderate effect.

The interlaminar stresses arise from difference of the ply CTEs in the longitudinal and transverse directions interaction between successive laminas, i.e., is a consequence of the stacking sequence adopted.

2.1.3 Tool-Part Interaction and Mold Effects

The other main driving factor behind built-up residual stress are the differential strains between the mold and part, because of different thermal expansion coefficients.

The effects of residual stresses and shape distortions in laminates are attributed to significant non-uniform distributions of in-plane shear stresses, which arise from constraints imposed by the tool/part interface (NIELSEN, 2013).

In a thermal expansion during cure in patamars above glass transition temperature, the expected stresses behavior between successive plies are higher in plies closed to the tool interface than other away. During the process, as resin is not fully cured, successive plies may slide, generating a through-thickness gradients in the ply stress, which will locked-in upon curing. Upon laminate tool-removal the stress equilibrium no longer exists and all these stresses relieved will convey a warpage aspect to a laminate. The Figure 2.4 illustrates the process sequence described.

It is noteworthy to mention that the stacking sequence plays a significant role in warpage behavior due to the different thermal expansion coefficients between successive plies.

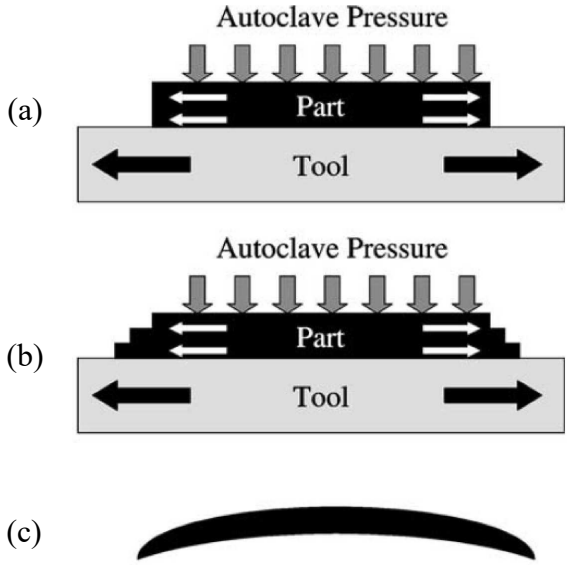

FIGURE 2.4 – Tool-part interaction effect in a VARTM process (a) Laminate stretched counter stiffer toll, (b) Interply-Slippage and (c) warpage resulting from demolding (Adapted from (NIELSEN, 2013)).

2.1.4 Other Factors

With less influence than the mechanisms previously described, it is worth to mention the cure cycle design, the composite thickness, the fiber volume fraction, void contents, and swelling caused by moisture. These elements must not be neglected when the objective is a high strength composite, like primary structures in aircraft.

Due to the viscoelastic nature of thermosets, for processes conducted at elevated temperatures, it is essential to employ a smart cure cycle that allows thermal expansion and shrinkage strains during curing to cancel each other out, thus effectively maintaining the matrix material volume somewhat constant, which helps reduce cure-induced strains (NIELSEN, 2013).

The composite thickness especially affects thermal gradients along thickness, significantly constraining cooling cure schedules due to the low thermal conductivity of thick composite sections.

Poor manufacturing control and wrong fiber volume fraction can lead to inhomogeneous distribution of fiber and matrix within a part. This significantly affects the resin flow in angle profiles curved sections and complex geometries, resulting in resin-rich or resin-poor regions.

Moreover, the void content requires special treatment, as its effect are relevant for the strength and fatigue life of composite laminate structures. Voids typically arise from entrapped air and moisture diffusion.

Therefore, aforementioned factors should not be neglected in the design strategy for manufacturing special composite, aiming to fully cover the residual stress prevention.

2.2 Modelling Approaches.

2.2.1 Micromechanics-Based Models

Micromechanics-based models have been extensively investigated recently. The work proposed by Chen (CHEN; ZHANG, 2018) explores residual stress in fiber-reinforced polymer matrix composites accounting for the thermal transfer in a microscale to compute curvature in thin plates. This model was applied to predict the cure-induced warpage of a non-symmetric laminate, comparing it with experimental results. A multi-physics and multi-scale approach was employed to model the composite as discrete layers in a macroscale, while micromechanics-model was implemented at the subscale based on fiber and matrix properties to compute effective lamina responses. The micromechanics rule used follows concentric cylinder assemblage of fiber-matrix pairs, as illustrated in Figure 2.5, and incorporates a cure-dependent constitutive law for resin cure kinetics.

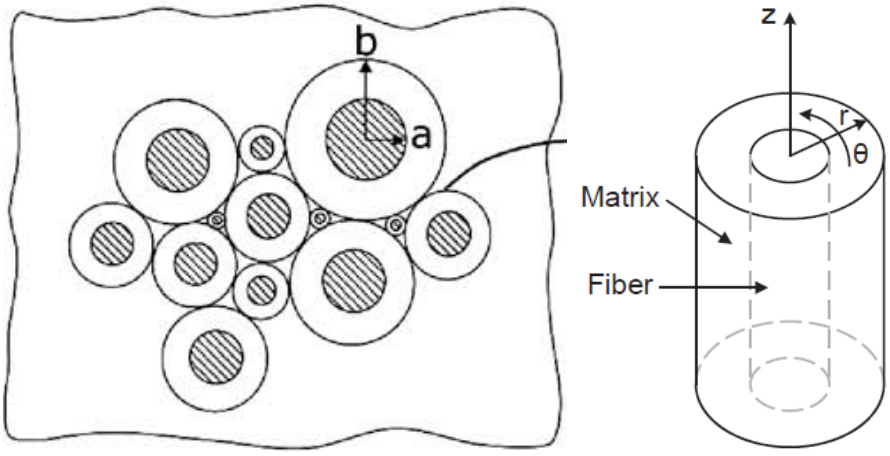

FIGURE 2.5 – Concentric cylinder assemblage of fiber-matrix pairs for a micromechanics-based model (Adapted from (CHEN; ZHANG, 2018)).

In this study simulations were also conducted to demonstrate temperature gradients through-the-thickness to evidence the interlaminar effect of different thermal expansion coefficients between successive laminas in thick laminates.

Additionally, model results were verified using frictional contact in ABAQUS® to simulate tool-part interaction, accounting for relative motion between the laminate and the mold, comparing the obtained experimental and numerical curvatures. In this scenario, the results perfectly match, evidencing the successfully predictions of the model. One conclusion drawn from this study is that the analysis solely based on the CLT approach overestimate results as it does not account for resin shrinkage and tool-part interaction.

In other recent work, Makinde (MAKINDE, 2018) demonstrates the influence of this residual stresses in angled structures and for singly curved sections, using a micromechanical based model integrated with path-dependent curing kinetics to predict shape distortions considering important mechanisms such as thermal expansion, resin shrinkage and frozen-in strains developed during curing cycles. Makinde's research also incorporates the chemical effects of resin in numerical simulations, which were further validated experimentally using carbon and glass hybrid laminates.

As a result, thickness variation effects were assessed on shape distortions and twist for a wing planform. One conclusion drawn was that these deformations are predominantly influenced by values along the longitudinal direction and along the out-of-plane transverse direction of laminate. Notably, CTE plays a primary role, followed by the resin rich zones, which can create stress concentration, especially on one side of the curved section. These factors have a significant impact on shape distortions, more than manufacturing quality or thickness of part.

2.2.2 Interlaminar Analytical Models

In a different vein, some researchers developed analytical models to capture interlaminar stresses rather than intralaminar ones. Yuan *et al.* (YUAN *et al.,* 2016) focused his study on interlaminar stresses and developed a model to predict through-the-thickness stresses and warpage in composite laminates during the autoclave curing process. The study highlights the critical impact of mismatches in the coefficient of thermal expansion (CTE) between the tool and composite materials, which generate significant interfacial shear stresses since the tool material has much higher CTE than the composite. These stresses affect the laminate's tension and warpage, with the model specifically addressing interlaminar stresses as key factors in

warpage and residual stresses. The model aims to predict how CTE differences between the tool and composite part influence the final product's shape and structural integrity.

The approach proposed by the authors simplifies the prediction of through-thickness stress distribution and warpage by assuming a constant interfacial shear stress along the tool-part interface, as illustrated in Figure 2.6 below, thereby circumventing the need for extensive resin characterization. It is assumed that plies close to the tool are stretched more than the plies further away, creating a stress gradient through the thickness of the laminate, similarly to a classical beam theory where the geometry undergoing tractions at the top and compressions at the bottom surfaces.

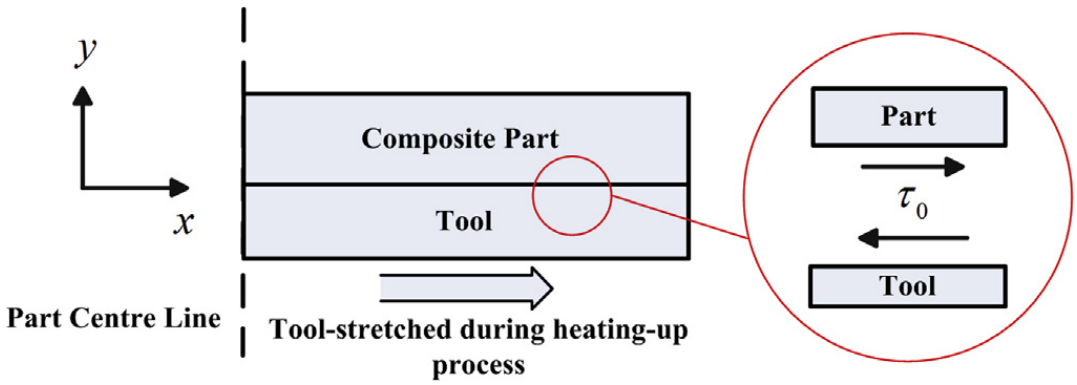

FIGURE 2.6 – Schematic of a composite part under sliding friction conditions due to tool expansion (Adapted from (YUAN *et al.,* 2016)).

This methodology leverages classical beam theory as a fundamental principle to enhance the predictive capabilities of closed-form solutions, thereby avoiding the complexities associated with cure kinetics and nonlinear material behavior.

The residual stress and warpage of composite part verified by the analytical model were validated against simulations using the Finite Element Method (FEM) with ABAQUS and experimental data, which are used to calibrate the input parameters of the approach. Results from the model show that warpage increases linearly with the increase in interfacial shear stress, emphasizing the critical need to account for stresses induced by tool-part interactions.

According to the author, the model not only demonstrates good agreement with experimental data but also provides a less computationally intensive alternative to FEM. It shows that the bending moment causing warpage is not solely due to residual stress induced in the plies, but also to the through-thickness stress distribution, which plays a significant role. This study highlights the essential management of these interactions to improve the quality and

dimensional accuracy of composite manufacturing processes, especially in scenarios involving autoclave curing with prepregs.

González-Cantero (GONZÁLEZ-CANTERO *et al.*, 2016) presents a novel analytical model for evaluating interlaminar stresses in curved composite laminates, specifically targeting scenarios of unfolding failure. This model focuses particularly on areas of high curvature in structures such as L-shaped, C-shaped, X-shaped, or T-shaped beams, where interlaminar stresses pose significant risks of delamination and subsequent failure. The methodology introduced by authors employs a set of infinite fictitious laminas in a 2D stress state assumption, improving the accuracy in predicting stresses compared to previous methods that struggled with the complexities of non-uniform loads and changes in curvature. Their results were validated against finite element models and literature for specific problems of curved section, demonstrating excellent agreement, and highlighting the model's effectiveness in managing complex load scenarios in beams with curved sections, considering the heterogeneity of a composite laminate across the thickness.

The study emphasizes interlaminar stresses as a critical factor in structural failures, particularly in unfolding failures in curved composite laminates subjected to normal and tangential loads. It was noted that areas of high curvature, such as in L-shaped or C-shaped beams, are particularly susceptible to delamination due to these stresses, which reflect the complexities arising from manufacturing processes and operational stresses in curved laminates, even knowing that interlaminar strengths are significantly lower than intralaminar strengths, which contributes to the emergence of undesirable failure modes.

Although both studies, carried out by Yuan *et al.* (YUAN *et al.*, 2016) and González-Cantero *et al.* (GONZÁLEZ-CANTERO *et al.,* 2016), emphasize the presence of interlaminar stresses and the importance of modeling them, Cantero et al. focused on the operational challenges posed by complex geometries employed in aircraft structures. They discussed the presence of interfacial stresses in these components and how the increase in interlaminar stresses contributes to the risk of delamination and unfolding failures. Conversely, Yuan *et al.* (YUAN *et al.*, 2016) demonstrated the significant impact of CTE mismatches on the interlaminar stresses in composites, evidencing that these CTE mismatches during the manufacturing process induce interfacial shear stresses and warpage. Thus, it was highlighted the importance of managing these mismatches to prevent residual stresses and deformation, through understanding and controlling CTE mismatches, aiming to enhance the structural integrity and performance of composite materials.

2.2.3 Variational Based Methods

Despite the particularities of constitutive behavior to any continuous body, either linear or non-linear material (REDDY, 2019) and its micromechanical modelling, other solutions can be obtained from powerful approaches employed in mechanic of structures like the direct variational methods as principles of virtual work and the principle of minimum total potential energy. These methods are based on stored energy within the system and work performed on it, allowing to obtain the set of equilibrium equations which leads to closed-form solutions for a few structures of relatively simple shape (ALLEN; HAISLER, 1985) and specific boundary conditions. However, for the majority of the structures, approximation functions are required to describe the strain-displacement relationships.

The key to use these principles is the easiness to determine approximate solutions of problems by employing a functional approach. Particularly with the total potential energy method, the solution is taken when the extremum (minimal and maximum) stationary values are found with respect to the variables of the problem (REDDY, 2004).

A very popular type of approximated solution method, which use these energy principles, is Rayeigh-Ritz, a technique for solving statically indeterminate structures, which can be used to treat the problem in terms of stresses and strains by solving a static equilibrium equation derived from the system's total energy (ALLEN; HAISLER, 1985). This technique is flexible and straightforward to apply because the functional includes all intrinsic features of the problem, such as the governing equations, boundary and/or initial conditions, and any constraints (REDDY, 2004), consisting in a basis for the development of displacement finite element models. Additionally, refining results can be achieved by increasing the number of functions in polynomial equation chosen for approximation, since the displacement field are consistent with the geometric constraints.

The other most popular and widely used approximation method is the Finite Element Methods, an approach derived from the Rayeigh-Ritz method. In FEM technique a given domain is viewed as an assemblage of subdomains (i.e., finite elements), and the displacement field of each subdomain could be described by base functions from a defined vectorial space (ELISEU LUCENA, 2021). The approximated solution is sought by locally admissible polynomial functions, which are piecewise smooth only over each individual subdomain (BARDELL, 1991). In FEM, also it is possible to easily input different boundary conditions. Accuracy of results can be achieved by enhanced the number of subdomains and/or choice of polynomial order of approximation of the elements.

3 Semi-Analytical Model Formulation

Based on these theories, this study aims to investigate a newly developed semi-analytical model for simulating fundamental geometric components in structural mechanics, such as laminated plates and plate-like beams, under different boundary conditions and loads, by utilizing engineering properties and material characterization parameters, such as coefficients of thermal expansion. This model streamlines the design concept step and prevents material losses during final assembly.

The proposed methodology is based on the computation of thermal residual strain-stresses, and the approach is addressed by the variational method of Principle of Stationary of the Total Potential Energy (PSTPE). The potential energy is minimized regarding the Rayleigh-Ritz Approximation Solution and using the Hierarchical Polynomial Bardell Functions to obtain the displacement field relations (BARDELL, 1991). The displacement field was assumed smoothly continuous along the thickness, following the use of the two-dimensional displacement-based formulation known as the Classical Laminate Theory (LIMA *et al.*, 2018).

3.1 Thermal Residual Strains and Stresses

As previously discussed, during the fabrication process of high-performance composite parts, processing thermoset resin at higher temperatures can often lead to increased residual stresses (ABOUHAMZEH *et al.*, 2019). Since laminates have been cured at different temperatures from the service temperature, thermal stresses arise and must be considered (JONES, 1999). Also, the inherent interaction between the laminate and the tool part, as well the complex chemical compatibility between layers in hybrid laminates due to the different CTE of materials, possess a challenge for design, even in a flat laminate manufacturing, where such thermal stress can be present, resulting in warpage as illustrated in Figure 3.1.

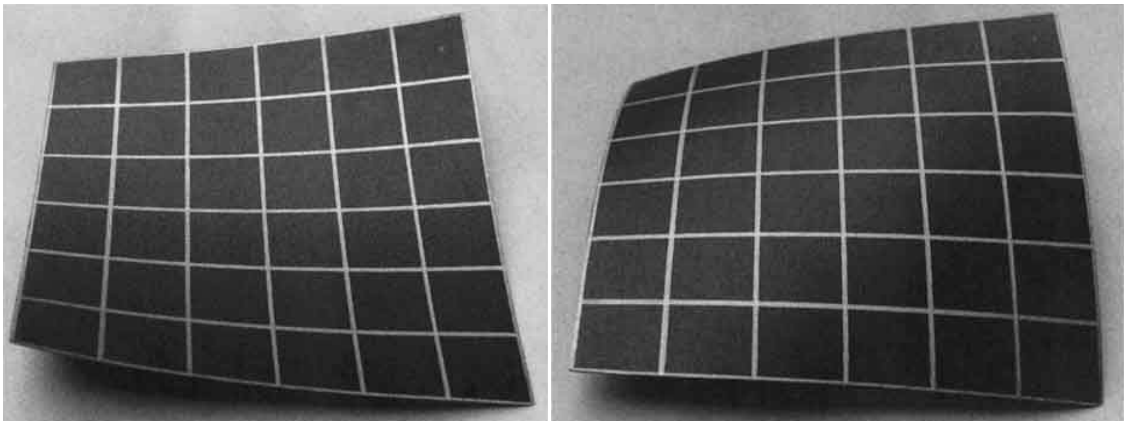

FIGURE 3.1 – Warpage of [20_2/-20_2] carbon/epoxy laminate (AS4/3501-6) (Adapted from (DANIEL; ISHAI, 2006)).

Therefore, thermal analysis can address more effects on laminate behavior than anticipated, being necessary to analyze the problem regarding thermoelastic effects. According to Daniel (DANIEL; ISHAI, 2006), the total strains in a laminate can be computed as an additive decomposition, i.e., the sum of all involved strains, as well as thermal effects, as given by Equation 1:

$$\{\boldsymbol{\varepsilon}\} = [\mathbf{S}]\{\boldsymbol{\sigma}\} + \Delta T\{\boldsymbol{\alpha}\} \tag{1}$$

The total strain $\{\boldsymbol{\varepsilon}\}$ consists of the mechanical strain term $[\mathbf{S}]\{\boldsymbol{\sigma}\}$, which relates to the constitutive material response to mechanical loads, and the last term $\Delta T\{\boldsymbol{\alpha}\}$, which relates to the thermal strains and requires knowledge of the thermal expansion coefficients. Considering a single orthotropic layer, conventionally referred to as the *k* layer, the total strains can be analyzed in its principal coordinate system (1, 2 and 3 directions), as Equation 2:

$$\begin{Bmatrix} \varepsilon_1 \\ \varepsilon_2 \\ \gamma_{12} \end{Bmatrix}_k = \begin{bmatrix} S_{11} & S_{12} & 0 \\ S_{12} & S_{22} & 0 \\ 0 & 0 & S_{66} \end{bmatrix}_k \begin{Bmatrix} \sigma_1 \\ \sigma_2 \\ \tau_{12} \end{Bmatrix}_k + \Delta T \begin{Bmatrix} \alpha_1 \\ \alpha_2 \\ 0 \end{Bmatrix}_k \tag{2}$$

where terms S_{ij} in flexibility matrix ($[\mathbf{S}]$) are related to the engineering properties of material of the layer, and α_1, α_2 are the longitudinal and transversal coefficients of thermal expansion in the principal laminae coordinate system. To determine the lamina stresses, Equation 2 must be inverted, leading to Equation 3:

$$\{\boldsymbol{\sigma}\}_k = [\mathbf{Q_b}]_k(\{\boldsymbol{\varepsilon}\}_k - \Delta T\{\boldsymbol{\alpha}\}_k) \tag{3}$$

Where, based on the constitutive relationship for laminae material, the matrix $[\mathbf{Q_b}]_k$ is given by Equation 4:

$$[\mathbf{Q_b}]_k = \begin{bmatrix} Q_{11} & Q_{12} & 0 \\ Q_{12} & Q_{22} & 0 \\ 0 & 0 & Q_{66} \end{bmatrix}_k = [\boldsymbol{S}]_k{}^{-1} \tag{4}$$

The terms of the constitutive matrix $[\boldsymbol{Q_b}]$ are function of engineering material properties for an orthotropic lamina, indicated by Equation 5:

$$\begin{gathered} Q_{11} = \frac{E_1}{1 - \upsilon_{12}\upsilon_{21}} \\ Q_{22} = \frac{E_2}{E_1} Q_{11} \\ Q_{22} = \frac{E_2}{E_1} Q_{11} \\ Q_{12} = \upsilon_{21} Q_{11} \\ Q_{66} = G_{12} \end{gathered} \tag{5}$$

In Equation 5 the constant E_1 represents the longitudinal Elastic Modulus, E_2 the transversal Elastic Modulus, υ_{12} the major Poisson´s ratio, υ_{21} the minor Poisson´s ratio and G_{12} the shear modulus at 1-2 plane. By changing the reference to an arbitrary coordinate system, (e.g., stresses described in a global x-y-z coordinate system), the total stresses for the *k* layer results as presented in Equation 6.

$$\begin{Bmatrix} \sigma_x \\ \sigma_y \\ \tau_{xy} \end{Bmatrix}_k = \begin{bmatrix} \bar{Q}_{11} & \bar{Q}_{12} & \bar{Q}_{16} \\ \bar{Q}_{12} & \bar{Q}_{22} & \bar{Q}_{26} \\ \bar{Q}_{16} & \bar{Q}_{26} & \bar{Q}_{66} \end{bmatrix}_k \left(\begin{Bmatrix} \varepsilon_x \\ \varepsilon_y \\ \gamma_{xy} \end{Bmatrix}_k - \Delta T \begin{Bmatrix} \alpha_x \\ \alpha_y \\ \alpha_{xy} \end{Bmatrix}_k \right) \tag{6}$$

In which the constitutive transformed matrix $[\overline{\boldsymbol{Q}}_b]_k$ for the *k* layer is given by Equation 7:

$$[\overline{\boldsymbol{Q}}_b]_k = [\boldsymbol{T}]_k{}^{-1} [\boldsymbol{Q_b}]_k \, [\boldsymbol{T}]_k{}^{-T} \tag{7}$$

calculate from the coordinate transformation matrix $[\boldsymbol{T}]$ between the reference systems as presented in Equation 8.

$$[\boldsymbol{T}]_k = \begin{bmatrix} cos^2\theta_k & sen^2\theta_k & 2cos\theta_k sen\theta_k \\ sen^2\theta_k & cos^2\theta_k & -2cos\theta_k sen\theta_k \\ -cos\theta_k sen\theta_k & cos\theta_k sen\theta_k & cos^2\theta_k - sen^2\theta_k \end{bmatrix} \tag{8}$$

Where θ_k is the angle between the principal direction of each layer and the longitudinal direction in global system. The set of equations described above is useful in the definition of the stiffnesses of a multilayered laminate and stress analysis in any arbitrary orientation for each k^{th} constituent layer.

3.2 Strain and Stress Variation in a Laminate Thickness

Now, considering a stacking sequence of laminae, compound a laminate, as shown in Figure 3.2 below, where each lamina through the laminate thickness contributes to the resultant laminate stresses.

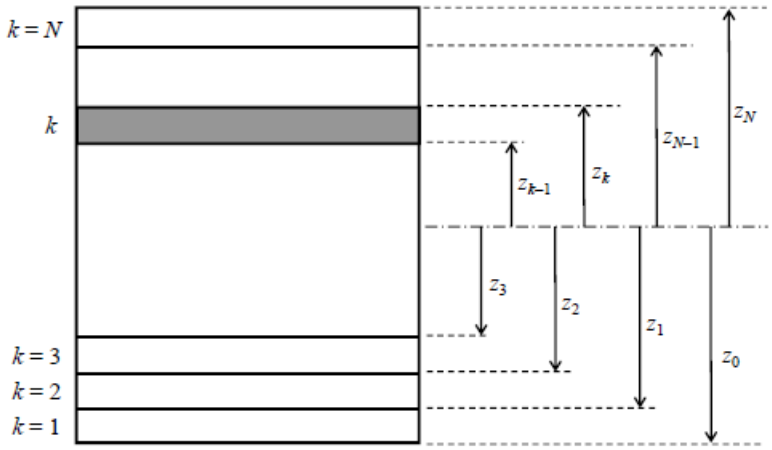

FIGURE 3.2 – A representative of a Stacking Sequence of laminas resulting in a laminate (Adapted from (DANIEL; ISHAI, 2006)).

Usually, according to the CLT analysis, the bonds between layers in a laminate are presumed to be infinitesimally thin and no-shear-deformable. The displacements are continuous across lamina boundaries, so that no lamina can slip relative to another, resulting in a stress distribution for each layer.

In a macroscale point of view, in a laminate with a representative stacking sequence of *N* laminas illustrated on Figure 3.2, there will be a similar stresses distribution computed as the sum of all laminae resultant stresses, as given by Equation 9:

$$\{\boldsymbol{N}\} = \sum_{k=1}^{N} \int_{z_{k-1}}^{z_k} \{\boldsymbol{\sigma}\}_k dz \tag{9a}$$

$$\{\boldsymbol{M}\} = \sum_{k=1}^{N} \int_{z_{k-1}}^{z_k} \{\boldsymbol{\sigma}\}_k z dz \tag{9b}$$

Each layer stresses and strains variation along laminate thickness (*t*) will contribute to a resultant laminate stresses and strains. The sum of those layer's stresses is referred to as generalized forces and moments, which now act on the laminae midplane, as shown in Figure 3.3, below:

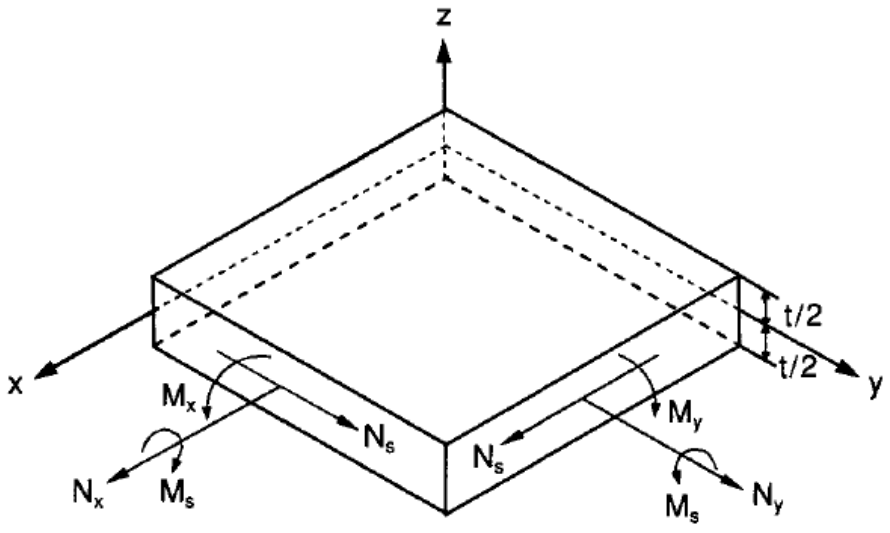

FIGURE 3.3 – A laminate with generalized forces and moments acting on its midplane, as a result of the layer stresses and strains variation through laminate thickness (Adapted from (DANIEL; ISHAI, 2006)).

From the Thin Plate theory, the assumption that each lamina exhibits small deflection behavior compared to the laminate dimensions, assures a Linear Strains-Displacements Relation (LSDR), illustrated in Figure 3.4.

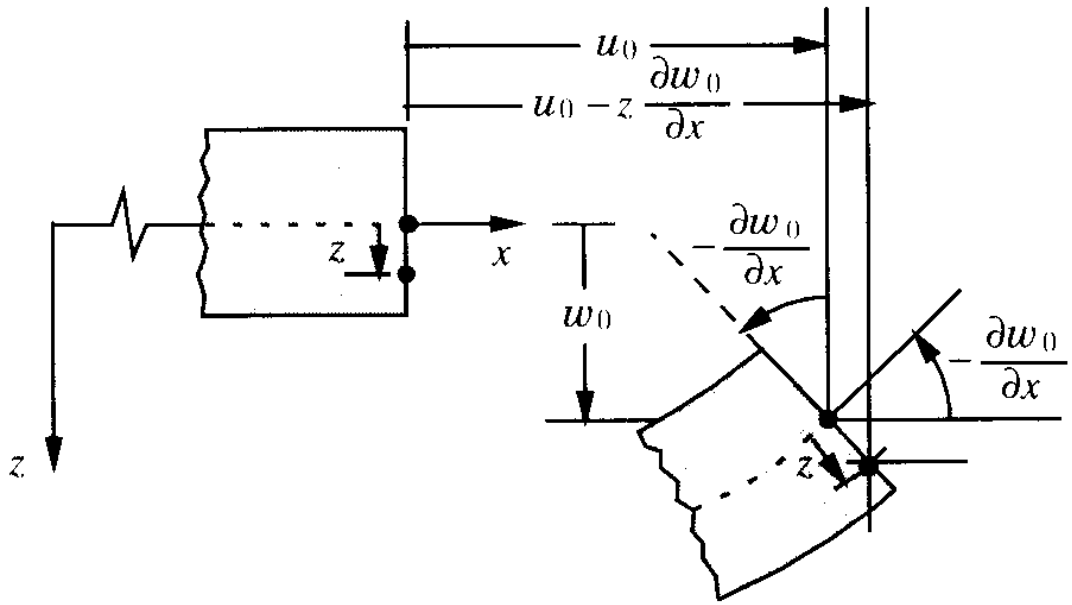

FIGURE 3.4 – Kinematics of thin lamina (Adapted from (REDDY, 2004)).

Assuming the rectangle in Figure 3.4 represents the cross-section of a laminate in a x-z or y-z plane, and the new position after the laminate undergoes a configuration change due to deformation by a stress gradient transformation, any arbitrary point in the deformed segment could be represented in terms of the plate middle plane displacements, and referred to laminate coordinate system, as given by Equation 10:

$$u(x,y,z) = u_0(x,y) - z\frac{\partial w_0(x,y)}{\partial x} \tag{10a}$$

$$v(x,y,z) = v_0(x,y) - z\frac{\partial w_0(x,y)}{\partial y} \tag{10b}$$

$$w = w_0(x,y) \tag{10c}$$

Therefore, the components of the linearized strain tensor at this point are given in Equation 11:

$$\varepsilon_x = \frac{\partial u(x,y,z)}{\partial x} = \frac{\partial u_0(x,y)}{\partial x} - z\frac{\partial^2 w_0(x,y)}{\partial x^2} = \varepsilon_x^0 + z\kappa_x \tag{11a}$$

$$\varepsilon_y = \frac{\partial v(x,y,z)}{\partial y} = \frac{\partial v_0(x,y)}{\partial y} - z\frac{\partial^2 w_0(x,y)}{\partial y^2} = \varepsilon_y^0 + z\kappa_y \tag{11b}$$

$$\gamma_{xy} = \frac{\partial u}{\partial y} + \frac{\partial v}{\partial x} = \frac{\partial u_0(x,y)}{\partial y} + \frac{\partial v_0(x,y)}{\partial x} - 2z\frac{\partial^2 w_0(x,y)}{\partial x \partial y} = \gamma_0 + z\kappa_{xy} \tag{11c}$$

Writing these strains-displacement relationship in a vector form results in Equation 12:

$$\begin{Bmatrix} \varepsilon_x \\ \varepsilon_y \\ \gamma_{xy} \end{Bmatrix} = \begin{Bmatrix} \dfrac{\partial u_0(x,y)}{\partial x} \\ \dfrac{\partial v_0(x,y)}{\partial y} \\ \dfrac{\partial u_0(x,y)}{\partial y} + \dfrac{\partial v_0(x,y)}{\partial x} \end{Bmatrix} + \mathrm{z}\begin{Bmatrix} -\dfrac{\partial^2 w_0(x,y)}{\partial x^2} \\ -\dfrac{\partial^2 w_0(x,y)}{\partial y^2} \\ -2\dfrac{\partial^2 w_0(x,y)}{\partial x \partial y} \end{Bmatrix} = \{\boldsymbol{\varepsilon}^0\} + z\{\boldsymbol{\kappa}\} \tag{12}$$

The vector $\{\boldsymbol{\varepsilon}^0\}$ is now referred to as midplane strain of laminate, while the vector $\{\boldsymbol{\kappa}\}$ as curvature.

Then, the laminae thermoelastic effects (Equation 6), accounted into laminate stresses' resultants (Equation 9), will give the generalized forces and moments acting in a mid-plane, as given by Equation 13:

$$\{\boldsymbol{N}\} = \begin{Bmatrix} N_x \\ N_y \\ N_{xy} \end{Bmatrix} = \sum_{k=1}^{N} \int_{z_{k-1}}^{z_k} [\overline{\boldsymbol{Q}}_b]_k \left(\begin{Bmatrix} \varepsilon_x^0 \\ \varepsilon_y^0 \\ \gamma_{xy}^0 \end{Bmatrix}_k + z\begin{Bmatrix} \kappa_x \\ \kappa_y \\ \kappa_{xy} \end{Bmatrix}_k - \Delta T \begin{Bmatrix} \alpha_x \\ \alpha_y \\ \alpha_{xy} \end{Bmatrix}_k \right) dz \tag{13a}$$

$$\{\boldsymbol{M}\} = \begin{Bmatrix} M_x \\ M_y \\ M_{xy} \end{Bmatrix} = \sum_{k=1}^{N} \int_{z_{k-1}}^{z_k} [\overline{\boldsymbol{Q}}_b]_k \left(\begin{Bmatrix} \varepsilon_x^0 \\ \varepsilon_y^0 \\ \gamma_{xy}^0 \end{Bmatrix}_k + z\begin{Bmatrix} \kappa_x \\ \kappa_y \\ \kappa_{xy} \end{Bmatrix}_k - \Delta T \begin{Bmatrix} \alpha_x \\ \alpha_y \\ \alpha_{xy} \end{Bmatrix}_k \right) z dz \tag{13b}$$

The contribution from the thermal effects can be evaluated as Equation 14:

$$\{\boldsymbol{N^T}\} = \begin{Bmatrix} N_x^T \\ N_y^T \\ N_{xy}^T \end{Bmatrix} = \sum_{k=1}^{N} \int_{z_{k-1}}^{z_k} [\overline{\boldsymbol{Q}}_b]_k \Delta T \begin{Bmatrix} \alpha_x \\ \alpha_y \\ \alpha_{xy} \end{Bmatrix}_k dz \tag{14a}$$

$$\{\boldsymbol{M^T}\} = \begin{Bmatrix} M_x^T \\ M_y^T \\ M_{xy}^T \end{Bmatrix} = \sum_{k=1}^{N} \int_{z_{k-1}}^{z_k} [\overline{\boldsymbol{Q}}_b]_k \Delta T \begin{Bmatrix} \alpha_x \\ \alpha_y \\ \alpha_{xy} \end{Bmatrix}_k z dz \tag{14b}$$

Where the $\{\alpha_x \quad \alpha_y \quad \alpha_{xy}\}^T$ is the vector containing the layer thermal coefficients calculated in the global coordinate system, as in Equation 15, based on its orientation θ_k :

$$\begin{Bmatrix} \alpha_x \\ \alpha_y \\ \alpha_{xy} \end{Bmatrix}_k = [\boldsymbol{T}]_k^{\,T} \begin{Bmatrix} \alpha_{1_k} \\ \alpha_{2_k} \\ 0 \end{Bmatrix} = \begin{Bmatrix} \alpha_{1_k}\cos^2(\theta_k) + \alpha_{2_k}\sin^2(\theta_k) \\ \alpha_{1_k}\sin^2(\theta_k) + \alpha_{2_k}\cos^2(\theta_k) \\ 2\cos(\theta_k)\sin(\theta_k)\left(\alpha_{1_k} - \alpha_{2_k}\right) \end{Bmatrix} \tag{15}$$

As the stiffness of each laminae constitutive relations can be calculated combining Equations 4, 5 and 7, Equation 13 could be rewritten as Equation 16:

$$\begin{Bmatrix} N_x \\ N_y \\ N_{xy} \end{Bmatrix} = \begin{bmatrix} A_{11} & A_{12} & A_{16} \\ A_{12} & A_{22} & A_{26} \\ A_{16} & A_{26} & A_{66} \end{bmatrix} \begin{Bmatrix} \varepsilon_x^0 \\ \varepsilon_y^0 \\ \gamma_{xy}^0 \end{Bmatrix} + \begin{bmatrix} B_{11} & B_{12} & B_{16} \\ B_{12} & B_{22} & B_{26} \\ B_{16} & B_{26} & B_{66} \end{bmatrix} \begin{Bmatrix} \kappa_x \\ \kappa_y \\ \kappa_{xy} \end{Bmatrix} - \begin{Bmatrix} N_x^T \\ N_y^T \\ N_{xy}^T \end{Bmatrix} \tag{16a}$$

$$\begin{Bmatrix} M_x \\ M_y \\ M_{xy} \end{Bmatrix} = \begin{bmatrix} B_{11} & B_{12} & B_{16} \\ B_{12} & B_{22} & B_{26} \\ B_{16} & B_{26} & B_{66} \end{bmatrix} \begin{Bmatrix} \varepsilon_x^0 \\ \varepsilon_y^0 \\ \gamma_{xy}^0 \end{Bmatrix} + \begin{bmatrix} D_{11} & D_{12} & D_{16} \\ D_{12} & D_{22} & D_{26} \\ D_{16} & D_{26} & D_{66} \end{bmatrix} \begin{Bmatrix} \kappa_x \\ \kappa_y \\ \kappa_{xy} \end{Bmatrix} - \begin{Bmatrix} M_x^T \\ M_y^T \\ M_{xy}^T \end{Bmatrix} \tag{16b}$$

The stiffness laminate matrices ($[\boldsymbol{A}]$, $[\boldsymbol{B}]$ and $[\boldsymbol{D}]$) are widely recognized as the integration of each lamina constitutive relationship, clearly demonstrated in open literature by Jones (JONES, 1999) and Daniel (DANIEL; ISHAI 2006). Thus, using the sum of mechanical and thermal generalized forces and moments applied on the laminate, it is possible to evaluate the thermoelastic effects over a laminate by rearranging Equation 16 above to find strains and, if necessary, curvatures at midplane of laminate by inverting this relation.

$$\begin{Bmatrix} \{\bar{\boldsymbol{N}}\} \\ \{\bar{\boldsymbol{M}}\} \end{Bmatrix} = \begin{Bmatrix} \{\boldsymbol{N^M}\} + \{\boldsymbol{N^T}\} \\ \{\boldsymbol{M^M}\} + \{\boldsymbol{M^T}\} \end{Bmatrix} = \begin{bmatrix} [\boldsymbol{A}] & [\boldsymbol{B}] \\ [\boldsymbol{B}] & [\boldsymbol{D}] \end{bmatrix} \begin{Bmatrix} \{\boldsymbol{\epsilon^0}\} \\ \{\boldsymbol{\kappa}\} \end{Bmatrix} \tag{17}$$

Or

$$\{\boldsymbol{f}\} = [\boldsymbol{C}]\{\boldsymbol{e}\} \tag{18}$$

Where the laminate has now a representative stiffness matrix given as,

$$[\boldsymbol{C}] = \begin{bmatrix} [\boldsymbol{A}] & [\boldsymbol{B}] \\ [\boldsymbol{B}] & [\boldsymbol{D}] \end{bmatrix} \tag{19}$$

Thus, by knowing of the generalized forces and moments applied to structures ($\{\bar{\boldsymbol{N}}\}$,$\{\bar{\boldsymbol{M}}\}$), whether they are mechanical ($\{\boldsymbol{N^M}\}$, $\{\boldsymbol{M^M}\}$), thermal ($\{\boldsymbol{N^T}\}$, $\{\boldsymbol{M^T}\}$) or a combination of both, by the geometric parameters of laminate and constitutive relations of layers, it is possible to determine the strains and curvature of mid-plane ($\{\boldsymbol{e}\}$).

3.3 Principle of Stationary of the Total Potential Energy (PSTPE)

Even though the stresses in an elastic body are unknown, the constitutive relations can be derived by expressing the equilibrium equations in terms of displacements rather than stresses, as demonstrated in the virtual work theorem. Therefore, this can be addressed by adopting the Principle of Stationary of the Total Potential Energy (PSTPE). PSTPE is a foundational concept in structural mechanics, providing an alternative basis for principles such as the Virtual Work theorem. It allows for deriving governing equations of continuum solids to directly determine exact or approximate solutions, intending to describe the system. Applicable across materials with linear or nonlinear elastic constitutive behavior (REDDY, 2019), PSTPE aims to solve the problem by finding the stationary values of a functional concerning the problem's variables. This functional is the total potential energy (Π) of the system, comprising the potential of internal energy due to deformation (U) and the potential of work done by external forces (V_E). The total potential energy is thus given by Equation 20 (REDDY, 2004):

$$\Pi = U + V_E \tag{20}$$

Analyzing this functional relative to a stationary point, the total potential energy of the system is minimum if its value is minimum at this point (MEGSON, 2015), yielding to equilibrium equations in terms of displacements for an elastic system, considering the internal strain energy (U) and external work done (W) over the system, as given by Equation 21.

$$\delta\Pi = \delta(U + V_E) = \delta(U - W) = 0 \tag{21}$$

Which may often be used to find approximated solutions for structural when an exact solution does not exist.

3.4 Rayleigh-Ritz Approximation Solution

According to Allen (ALLEN; HAISLER, 1985), exact solutions to boundary value problems are impractical for complex structural systems. However, a powerful technique within variational methods, the Rayleigh-Ritz method, addresses this challenge by providing approximate solutions. This method ensures equilibrium and geometric compatibility by solving static equilibrium equations in terms of scalar energy quantity, representing the total energy of the system (Π).

In the Rayleigh-Ritz method, displacement-fields are approximated using polynomial series with non-physical coefficients shown in Equation 22 below, referred to as generalized coordinates, i.e., $q_{ij}^{u,v,w}$. The polynomial approximation functions with respect to x and y coordinates, $\phi_i(x)$ and $\psi_j(y)$, satisfy essential geometric boundary problem conditions.

$$u_0(x,y) = \sum_{i=1}^{n}\sum_{j=1}^{m} q_{ij}^{u}\phi_i(x)\psi_j(y) = [\boldsymbol{N}^u(x,y)]\{\boldsymbol{q}^u\} \tag{22a}$$

$$v_0(x,y) = \sum_{i=1}^{n}\sum_{j=1}^{m} q_{ij}^{v}\phi_i(x)\psi_j(y) = [\boldsymbol{N}^v(x,y)]\{\boldsymbol{q}^v\} \tag{22b}$$

$$w_0(x,y) = \sum_{i=1}^{n}\sum_{j=1}^{m} q_{ij}^{w}\phi_i(x)\psi_j(y) = [\boldsymbol{N}^w(x,y)]\{\boldsymbol{q}^w\} \tag{22c}$$

Equation 22 can be represented in a matrix form where $[\boldsymbol{N}^{u,v\ or\ w}(x,y)]$ are the *1xnm* line matrices containing the form functions, resulted from all the products $\phi_i(x)\psi_j(y)$, i.e., $[\phi_1(x)\psi_1(y)\ \dots\ \phi_1(x)\psi_m(y)\ \phi_2(x)\psi_1(y)\ \dots\ \phi_2(x)\psi_m(y)\ \phi_n(x)\psi_1(y)\ \dots\ \phi_n(x)\psi_m(y)]$. And the *nmx1* column matrices $\{\boldsymbol{q}^{u,v\ or\ w}\}$ containing the generalized coordinates, $[q_{11}^u\ \dots\ q_{1m}^u\ q_{21}^u\ \dots\ q_{2m}^u\ q_{n1}^u\ \dots\ q_{nm}^u]^T$. Alternatively, Equation 23 can be written in matrix form as follows,

$$\begin{Bmatrix} u_0 \\ v_0 \\ w_0 \end{Bmatrix} = \begin{bmatrix} [\boldsymbol{N}^u(x,y)] & [0] & [0] \\ [0] & [\boldsymbol{N}^v(x,y)] & [0] \\ [0] & [0] & [\boldsymbol{N}^w(x,y)] \end{bmatrix} \begin{Bmatrix} \{\boldsymbol{q}^u\} \\ \{\boldsymbol{q}^v\} \\ \{\boldsymbol{q}^w\} \end{Bmatrix} \tag{23}$$

Or, briefly,

$$\{\boldsymbol{d}\} = [\boldsymbol{N}]\{\boldsymbol{q}\} \tag{24}$$

Considering that the strains in each lamina are given by the linear strain-displacement relationship, the mid-plane laminate strain $\{\boldsymbol{\varepsilon}^0\}$ and curvature $\{\boldsymbol{\kappa}\}$ can be represented in matrix form in Equation 25, using these approximations mentioned above and taking the first and second derivative with respect to coordinates *x* and *y*:

$$\begin{Bmatrix}\{\boldsymbol{\varepsilon}^0\}\\ \{\boldsymbol{\kappa}\}\end{Bmatrix} = \begin{Bmatrix}\varepsilon_x^0\\ \varepsilon_y^0\\ \varepsilon_{xy}^0\\ \kappa_x\\ \kappa_y\\ \kappa_{xy}\end{Bmatrix} = \begin{bmatrix}\begin{bmatrix}\boldsymbol{N}_{,x}^u(x,y)\end{bmatrix} & [0] & \begin{bmatrix}[0]\\ [0]\\ [0]\end{bmatrix}\\ [0] & \begin{bmatrix}\boldsymbol{N}_{,y}^v(x,y)\end{bmatrix} & \\ \begin{bmatrix}\boldsymbol{N}_{,y}^u(x,y)\end{bmatrix} & \begin{bmatrix}\boldsymbol{N}_{,x}^v(x,y)\end{bmatrix} & \\ \begin{bmatrix}[0] & [0]\\ [0] & [0]\\ [0] & [0]\end{bmatrix} & & \begin{bmatrix}\boldsymbol{N}_{,xx}^w(x,y)\\ \boldsymbol{N}_{,yy}^w(x,y)\\ 2\boldsymbol{N}_{,xy}^w(x,y)\end{bmatrix}\end{bmatrix}\begin{Bmatrix}\{\boldsymbol{q}^u\}\\ \{\boldsymbol{q}^v\}\\ \{\boldsymbol{q}^w\}\end{Bmatrix} \tag{25}$$

Or in a contracted form,

$$\{\boldsymbol{e}\} = [\boldsymbol{B}]\{\boldsymbol{q}\} \tag{26}$$

The Equation 26 above is useful when minimizing the Total Potential Energy to obtain the set of equilibrium equations.

3.5 Hierarchical Polynomial Bardell Functions

The set of functions used in the present work to describe the displacement-field approximations is derived from the Rodrigue's form of Legendre Orthogonal Polynomial's (BARDELL, 1991). The polynomial form defined by Bardel is showed in Equation 27 below:

$$f_r(\xi \; or \; \eta) = \sum_{n=0}^{r/2} \frac{(-1)^n(2r-2n-7)!!}{2^n n!\,(r-2n-1)!}(\xi \; or \; \eta)^{r-2n-1}, \qquad r > 4. \tag{27}$$

Where the non-dimensional coordinates are given by $\xi = {}^{2x}/_{a} - 1$ or $\eta = {}^{2y}/_{b} - 1$, and $r!! = r(r-2)$, and $0!! = (-1)!! = 1$, r is the number of functions chosen for the polynomial series, remembering that should be more than 4. If r is an odd number, the value of ${}^{r}/_{2}$ is taken as the integer part of this division result. The parameters a and b are the dimensions of length and width, respectively, for a flat plate element showed in Figure 3.5. This plate has discretized

as one whole element and the interval of the non-dimensional coordinates (also known as natural coordinates) ($\xi \; or \; \eta$) is $[-1,1]$ as showed in Figure 3.5.

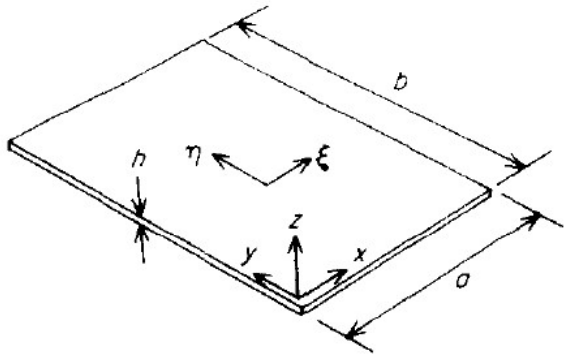

FIGURE 3.5 – An example of rectangular plate element with natural coordinates (Adapted from (BARDELL, 1991)).

The first ten Polynomials and their correspondent slopes can be verified in Bardell's (BARDELL, 1991) work. One important characteristic of these polynomials is that they belong to the same orthogonal basis of the Euler-Bernoulli beam element, as shown in Equation 28 bellow. Thus, for a plate element as in Figure 3.5, its degrees of freedom can be given by the first four polynomial's.

$$f_1(\xi \; or \; \eta) = \frac{1}{2} - \frac{3}{4}(\xi \; or \; \eta) + \frac{1}{4}(\xi \; or \; \eta)^3 \tag{28a}$$

$$f_2(\xi \; or \; \eta) = \frac{1}{8} - \frac{1}{8}(\xi \; or \; \eta) - \frac{1}{8}(\xi \; or \; \eta)^2 + \frac{1}{8}(\xi \; or \; \eta)^3 \tag{28b}$$

$$f_3(\xi \; or \; \eta) = \frac{1}{2} + \frac{3}{4}(\xi \; or \; \eta) - \frac{1}{4}(\xi \; or \; \eta)^3 \tag{28c}$$

$$f_4(\xi \; or \; \eta) = -\frac{1}{8} - \frac{1}{8}(\xi \; or \; \eta) + \frac{1}{8}(\xi \; or \; \eta)^2 + \frac{1}{8}(\xi \; or \; \eta)^3 \tag{28d}$$

These first four cubic modes of Bardell Polynomial's presented are related to edge degrees of freedom and are used to model the cases studied in the present work, such as the plate clamped at one of its edges. Figure 3.6 shows these four polynomials, where the edge effect can be seen. According to the rule, the first and third are related to the edge displacement, representing either free or clamped constraints. When observing the edge on the left side ($\xi = -1$), the first polynomial allows for free displacement ($f_1(\xi) = 1$), whilst the third polynomial imposes a

constraint ($f_3(\xi) = 0$). At the right side ($\xi = 1$), the first polynomial imposes a clamped displacement ($f_1(\xi) = 0$) and the third polynomial allows for free displacement ($f_3(\xi) = 1$).

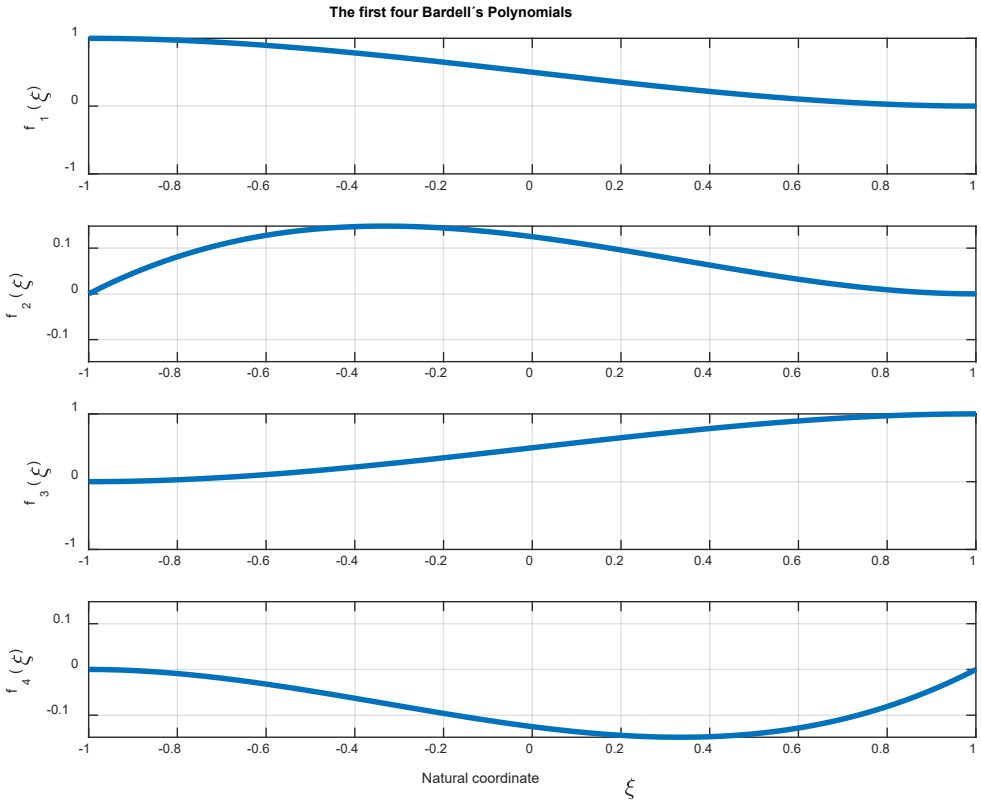

FIGURE 3.6 – The first four polynomials of Bardell´s Functions in natural coordinates, (Source Author).

The second and fourth polynomials are related to edge rotation. On the left side ($\xi = -1$), edge rotation is constrained by the fourth polynomial, while the second allows free rotation. On the right side ($\xi = 1$), the rotation constraint is opposite for these polynomials. This effect is illustrated in Figure 3.7, where the first derivative with respect to ξ of these first four polynomials are shown. On the left side ($\xi = -1$), the derivative function equals zero for the fourth polynomial and differs from zero for the second polynomial in the same side.

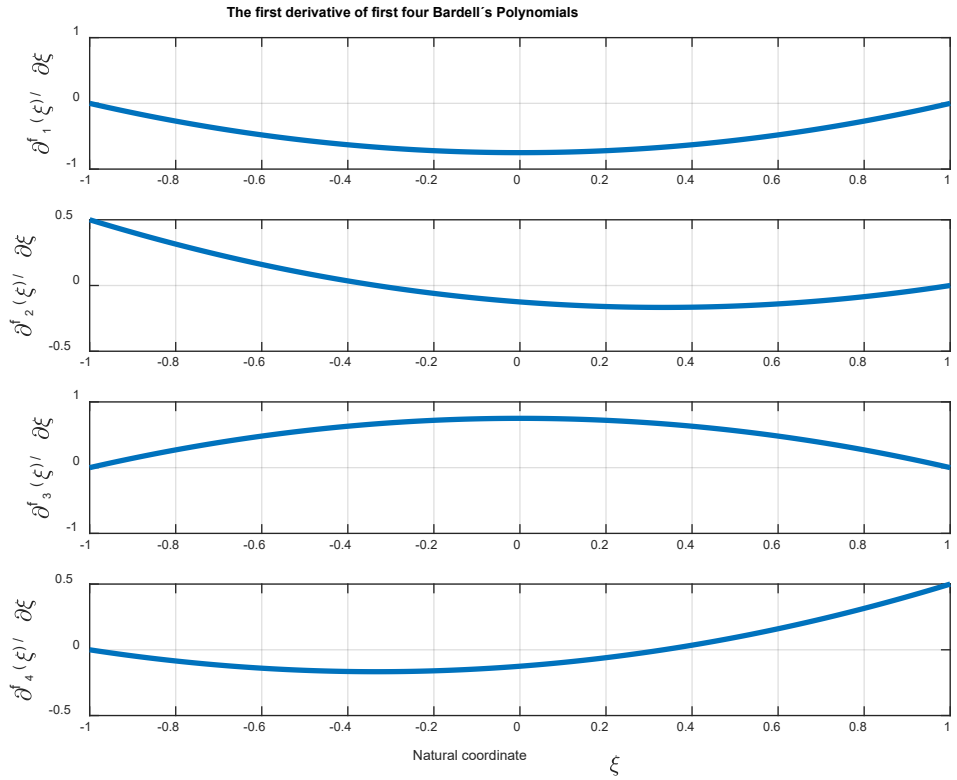

FIGURE 3.7 – The first derivative of the first four polynomials of Bardell´s Functions, in natural coordinates, (Source Author).

Starting from the fifth polynomial, all Bardell polynomials have no effect on the boundaries, allowing refinements without difficult in imposing boundary conditions. This approach guarantees satisfaction of the boundary conditions, and meets the minimum continuity requirement, simplifying the computation of displacements, strains and consequently stresses.

Therefore, the form functions indicated in Equation 22 can now be rewritten in non-dimensional coordinates ($\xi \; or \; \eta$). As an example, for the displacement field in u, (Equation 22a), the line matrix containing the form functions is as follows:

$$[\boldsymbol{N}^{u}(\xi,\eta)] = [f_1(\xi)f_1(\eta) \dots f_1(\xi)f_m(\eta) \;\; f_2(\xi)f_1(\eta) \dots f_2(\xi)f_m(\eta) \; f_n(\xi)f_1(\eta) \dots \; f_n(\xi)f_m(\eta)]$$

3.6 Proposed Semi-Analytical Model

Using the Bardell functions (Equations 27 and 28) to represent the displacement field given in Equation 22, we derive the set of equations in the three principal directions shown as presented in Equation 25. This leads to Equation 29, which describes the strains and curvatures:

$$\begin{Bmatrix}\{\boldsymbol{\varepsilon}^0\}\\ \{\boldsymbol{\kappa}\}\end{Bmatrix}=\begin{bmatrix} {}^{2}/_{a}\left[\boldsymbol{N}^{u}_{,\xi}(\xi,\eta)\right] & [0] & [0]\\ [0] & {}^{2}/_{b}\left[\boldsymbol{N}^{v}_{,\eta}(\xi,\eta)\right] & [0]\\ {}^{2}/_{b}\left[\boldsymbol{N}^{u}_{,\eta}(\xi,\eta)\right] & {}^{2}/_{a}\left[\boldsymbol{N}^{v}_{,\xi}(\xi,\eta)\right] & [0]\\ [0] & [0] & {}^{4}/_{a^2}\left[\boldsymbol{N}^{w}_{,\xi\xi}(\xi,\eta)\right]\\ [0] & [0] & {}^{4}/_{b^2}\left[\boldsymbol{N}^{w}_{,\eta\eta}(\xi,\eta)\right]\\ [0] & [0] & {}^{8}/_{ab}\left[\boldsymbol{N}^{w}_{,\xi\eta}(\xi,\eta)\right]\end{bmatrix}\begin{Bmatrix}\{\boldsymbol{q}^{u}\}\\ \{\boldsymbol{q}^{v}\}\\ \{\boldsymbol{q}^{w}\}\end{Bmatrix} \tag{29}$$

Thus, by minimizing the total potential energy (Π) defined in Equation 21, we obtain the following expression,

$$\delta\Pi=\{\delta\boldsymbol{q}\}^{T}\frac{\partial\Pi}{\partial\{\boldsymbol{q}\}}=0 \tag{30}$$

for the plate under thermo-mechanical loads, the minimal functional Π will result:

$$\delta\Pi=\{\delta\boldsymbol{q}\}^{T}\left(\int_{S}[\boldsymbol{B}]^{\boldsymbol{T}}[\boldsymbol{C}][\boldsymbol{B}]\,dS\{\boldsymbol{q}\}-\int_{S}[\boldsymbol{B}]^{\boldsymbol{T}}\{\boldsymbol{f}\}\,dS-\int_{S}[\boldsymbol{N}]^{\boldsymbol{T}}\{\boldsymbol{f}_{\mathbf{S}}\}\,dS-\int_{\boldsymbol{\Gamma}}[\boldsymbol{N}]^{\boldsymbol{T}}\{\boldsymbol{f}_{\boldsymbol{\Gamma}}\}\,d\boldsymbol{\Gamma}-\sum_{\boldsymbol{i}}[\boldsymbol{N}]^{\boldsymbol{T}}\{\boldsymbol{f}_{\mathbf{i}}\}\right)=0$$

The above expression can be briefly written as follows,

$$\delta\Pi=\{\delta\boldsymbol{q}\}^{T}\left([\boldsymbol{K}]\{\boldsymbol{q}\}-\{\boldsymbol{F}_{\boldsymbol{f}}\}-\{\boldsymbol{F}_{\boldsymbol{S}}\}-\{\boldsymbol{F}_{\boldsymbol{\Gamma}}\}-\{\boldsymbol{F}_{\boldsymbol{i}}\}\right)=\mathbf{0} \tag{32}$$

Where $[\boldsymbol{K}]$ is the stiffness matrix of system, and $\{\boldsymbol{F}_{\boldsymbol{f}}\}$, $\{\boldsymbol{F}_{\boldsymbol{S}}\}$, $\{\boldsymbol{F}_{\boldsymbol{\Gamma}}\}$, $\{\boldsymbol{F}_{\boldsymbol{i}}\}$ refer to the vectors associated with the midplane generalized thermo-mechanical forces ($\{\boldsymbol{f}\}$), transverse force per unit of area ($\{\boldsymbol{f}_{\mathbf{S}}\}$) , transverse force per unit of length ($\{\boldsymbol{f}_{\boldsymbol{\Gamma}}\}$) and concentrated forces ($\{\boldsymbol{f}_{\mathbf{i}}\}$) acting on the laminate, respectively, schematically indicated in Figure 3.8,

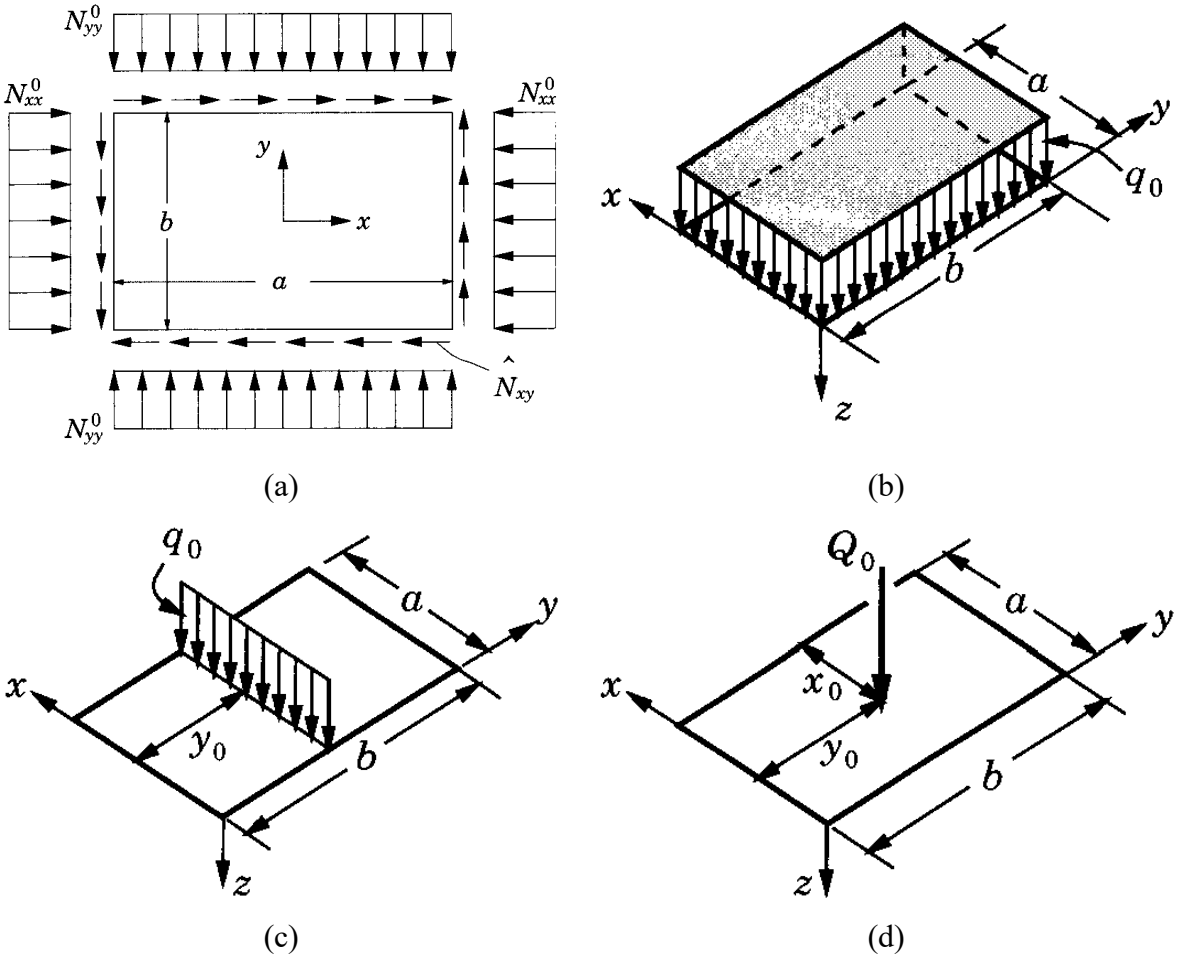

FIGURE 3.8 – An illustration of plate with (a) mid-plane generalized forces and moments (b) transverse load per unit of area, (c) load per unit of length, and (d) transverse concentrated force (Adapted from (REDDY, 2004)).

The stiffness matrix of the system, and the vectors associated with the forces indicated in Equation 32 are computed as follows,

$$[\boldsymbol{K}] = \int_S [\boldsymbol{B}]^T [\boldsymbol{C}][\boldsymbol{B}]\, dS \tag{33}$$

$$\{\boldsymbol{F_f}\} = \int_S [\boldsymbol{B}]^T \{\boldsymbol{f}\}\, dS \tag{34}$$

$$\{\boldsymbol{F_S}\} = \int_S [\boldsymbol{N}]^T \{\boldsymbol{f_S}\}\, dS \tag{35}$$

$$\{\boldsymbol{F_\Gamma}\} = \int_\Gamma [\boldsymbol{N}]^T \{\boldsymbol{f_\Gamma}\}\, d\boldsymbol{\Gamma} \tag{36}$$

$$\{\boldsymbol{F_i}\} = \sum_{\boldsymbol{i}} [\boldsymbol{N}]^{\boldsymbol{T}} \{\boldsymbol{f_i}\} \tag{37}$$

The vectors $\{\boldsymbol{f}\}$, $\{\boldsymbol{f_S}\}$, $\{\boldsymbol{f_\Gamma}\}$, and $\{\boldsymbol{f_i}\}$, indicated in Equations 34, 35, 36 and 37 are related to the forces applied over the laminate,

$$\{\boldsymbol{f}\} = \begin{Bmatrix} N_{xx}^0 \\ N_{yy}^0 \\ N_{xy}^0 \\ M_{xx}^0 \\ M_{yy}^0 \\ M_{xy}^0 \end{Bmatrix} \qquad \{\boldsymbol{f_S}\} = \begin{Bmatrix} f_{Sx} \\ f_{Sy} \\ f_{Sz} \end{Bmatrix} \qquad \{\boldsymbol{f_\Gamma}\} = \begin{Bmatrix} f_{\Gamma x} \\ f_{\Gamma y} \\ f_{\Gamma z} \end{Bmatrix} \qquad \{\boldsymbol{f_i}\} = \begin{Bmatrix} f_{ix} \\ f_{iy} \\ f_{iz} \end{Bmatrix}$$

The non-trial solution of Equation 32 results in the following set of linear equations to be solved,

$$[\boldsymbol{K}]\{\boldsymbol{q}\} = \{\boldsymbol{F_f}\} + \{\boldsymbol{F_S}\} + \{\boldsymbol{F_\Gamma}\} + \{\boldsymbol{F_i}\} \tag{38}$$

The solution of linear system given in Equation 38 allows for the determination of the generalized coordinates $\{\boldsymbol{q}\}$, as indicated in Equation 39,

$$\{\boldsymbol{q}\} = [\boldsymbol{K}]^{-1}\left(\{\boldsymbol{F_f}\} + \{\boldsymbol{F_S}\} + \{\boldsymbol{F_C}\} + \{\boldsymbol{F_i}\}\right) \tag{39}$$

Consequently, we obtain the displacements and strains through Equations 24 and 26, respectively, which are reiterated:

$$\{\boldsymbol{d}\} = [\boldsymbol{N}]\{\boldsymbol{q}\} \tag{24}$$

$$\{\boldsymbol{e}\} = [\boldsymbol{B}]\{\boldsymbol{q}\} \tag{26}$$

Yielding to the determination of any residual stress layer by using the equation 3, repeated here, and allowing for analysis.

$$\{\boldsymbol{\sigma}\}_k = [\mathbf{Q_b}]_k(\{\boldsymbol{\varepsilon}\}_k - \Delta T\{\boldsymbol{\alpha}\}_k) \tag{3}$$

Thus, the proposed semi-analytical model can now be applied to plates and plate-like beam geometries of laminates under generalized thermo-mechanical forces acting in its midplane, as well as mechanical forces either applied transversely per unit of area, per unit of length or concentrated.

All vectors and matrices related to Equation 38 were implemented in a computing environment using the commercial platform MATLAB®, considering different laminates, geometries, boundary conditions and loads. The results are presented in the next chapter.

4 Results and Discussion

The purpose of this chapter is to describe the results obtained using the proposed semi-analytical model, which employs Bardell´s functions to approximate displacement-fields in the Rayleigh-Ritz approximation solution for the thermoelastic loads in laminate plate-like beam and plate composites.

Initially, the model was implemented to solve common problems found in the open literature for different load cases, such as cantilever plate-like beam with mechanical load, in configurations as, load at tip, distributed load, and for a biclampled plate-like beam with load at middle, considering an E-glass Epoxy laminate.

Next, a Carbon-Fiber composite free plate $[90_2/0_2]$ was considered, and simulations were carried out under thermal loads only, as this layup exhibits warpage under thermal loading. Additionally, the results were compared with an equation for CLT warpage solution found in Daniel (DANIEL; ISHAI, 2006). To verify the model effectiveness, a stress analysis was carried out, and the principal stresses were computed for each layer in the laminate. The sum of these stresses equals zero, confirming the model accuracy for thermal load conditions.

Furthermore, a bi-material clamped plate-like beam was verified under thermal load, and the results were compared with an exact solution equation of a bi-material experiment, available in Cambridge University website (THERMAL, 2022).

Finally, the proposed semi-analytical model was used to verify the thermal load in a monolithic composite plate, simulating a cure step that occurs in composite fabrication. In this case, the result was compared with simulation using the software ABAQUS®.

4.1 Verification of the Proposed Semi-Analytical Model for Mechanical Loading Cases

4.1.1 Case 1: Cantilever Composite Plate-Like Beam with a Concentrated Load at the Tip

The semi-analytical model previously presented was implemented and validated against three well know literature cases, considering mechanical load only.

Firstly, a punctual mechanical load was applied to the tip of a cantilever beam, as shown in Figure 4.1. The maximum deflection obtained from the closed-form solution of the problem is also indicated in the figure.

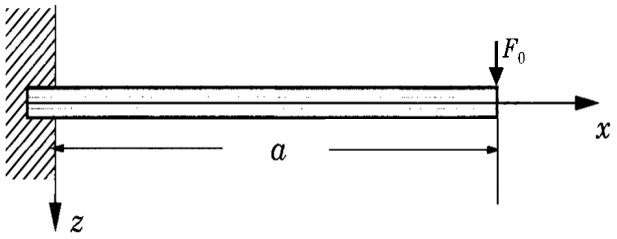

$$w_{tip} = \frac{F_0 a^3}{3EI}$$

FIGURE 4.1 – An example of cantilever beam loaded at the tip, along with the equation from closed-form solution to compute the maximum deflection (Adapted from (REDDY, 2004)).

A unidirectional laminate [0_9] was chosen to facilitate the effective laminate Young´s Moduli ($\bar{E}_x$) computation and to allow the comparison with the closed-form solution. The lamina properties are listed in Table 4.1 below, with geometry values of length $a = 254\,mm$, width $b = a/20$ and thickness $t = 0.127\,mm$, resulting in a plate-like beam geometry. A E-Glass/Epoxy laminate was chosen because this material has the extensive data available in literature, which allows the reader to verify the information.

TABLE 4.1 – Engineering properties of laminae for E-Glass/Epoxy, from (JONES, 1999).

$\boldsymbol{E_1}$ [MPa]	$\boldsymbol{E_2}$ [MPa]	$\boldsymbol{\upsilon_{12}}$	$\boldsymbol{G_{12}}$ [MPa]	$\boldsymbol{\alpha_1}$ [°C^{-1}]	$\boldsymbol{\alpha_2}$ [°C^{-1}]
53780	17930	0.25	8620	6.3x10^{-6}	20.52x10^{-5}

The result for the maximum deflection using the closed-form solution indicated in Figure 4.1 was computed using the effective laminate Young´s Moduli ($\bar{E}_x$) calculated following the section 7.12 in Daniel (DANIEL; ISHAI, 2006). The Moment of Inertia depends on the rectangular geometry section ($I = b.h^3/12$) and the applied mechanical load was $F_0 = 1N$ in z-direction. The maximum deflection result for closed-formed solution is $w_{max} = 64.2685\,mm$.

Employing the proposed semi-analytical model, the typical deflection result is obtained by taken the Equation 38, where the laminate is under concentrated load forces, represented by the vector $\{\boldsymbol{f_i}\} = \{0 \quad 0 \quad F_0\}^T$, resulting in the equilibrium set of equations $[\boldsymbol{K}]\{\boldsymbol{q}\} = \{\boldsymbol{F_i}\}$.

The solution of this system provides the column matrix $\{\boldsymbol{q}\}$, containing the generalized coordinates. The maximum deflection w_{max} is then computed using Equation 24. The displacement field and the w_{max} are shown in Figure 4.2. The geometric boundary conditions assured by Bardell functions combination was (Clamped-Free-Free-Free), using the third and fourth polynomials in the ξ coordinate and all the first four polynomials in the η coordinate. The result of $w_{max} = 64.1566\ mm$ was obtained using 15 terms in the polynomial Bardell series in the x and y directions.

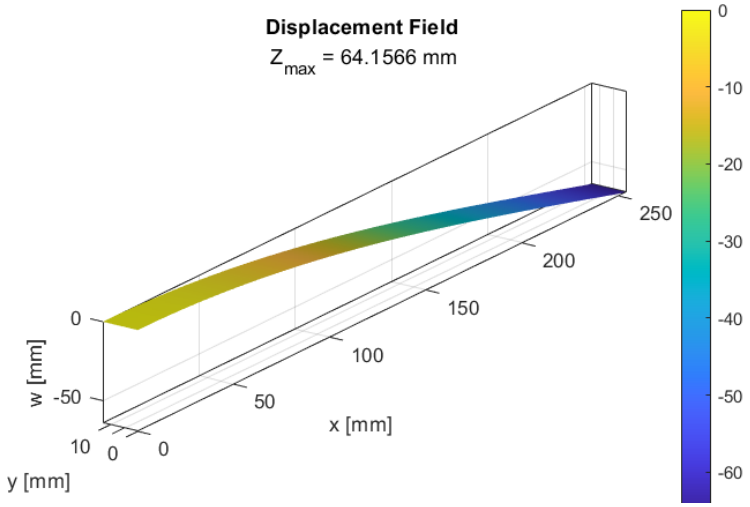

FIGURE 4.2 – The cantilever beam simulated using the proposed semi-analytical model.

4.1.2 Case 2: Cantilever Composite Plate-Like Beam with Distributed Load

Next, the proposed semi-analytical model is verified by using a distributed mechanical load of $q_0 = 1\ \mathrm{N}/mm$ in z-direction as shown in the Figure 4.3, applied to the previously described cantilever beam. The problem given by Equation 38 results now in the set of equilibrium equations $[\boldsymbol{K}]\{\boldsymbol{q}\} = \{\boldsymbol{F_\Gamma}\}$, with transverse force per unit of length acting in the laminate as the vector $\{\boldsymbol{f_\Gamma}\} = \{0 \quad 0 \quad q_0\}^T$. The geometric boundary conditions ensured by the combination of Bardell functions were the same as in the previous problem (Clamped-Free-Free-Free), using the third and fourth polynomials in the ξ coordinate and all the first four polynomials in the η coordinate.

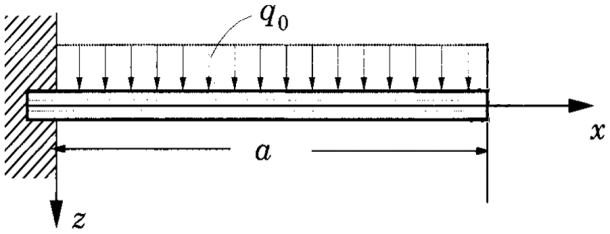

$$w_{tip} = \frac{q_0 a^4}{8EI}$$

FIGURE 4.3 – A cantilever beam with distributed load and the expression for maximum deflection (Adapted from (REDDY, 2004)).

The deflection obtained through the closed-form solution is $w_{tip} = 24.1007\ mm$. Figure 4.4 shows the beam deflection and its maximum value (w_{max}) obtained through simulation of the proposed semi-analytical model using 15 terms in the polynomial Bardell series in the x and y directions.

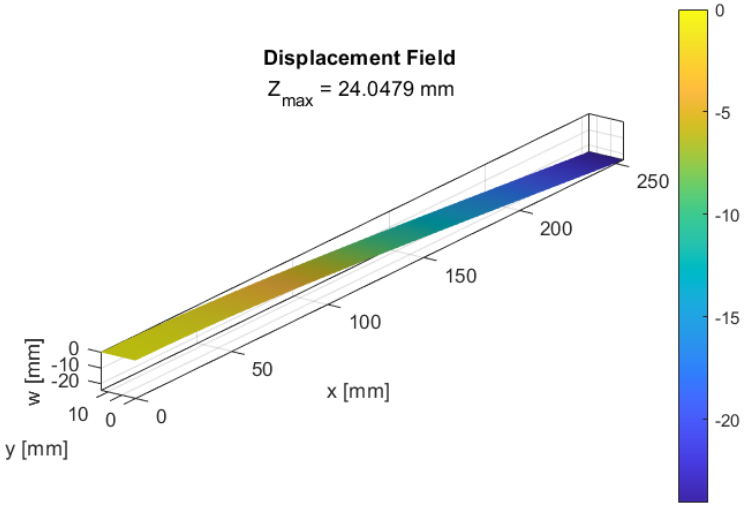

FIGURE 4.4 – The cantilever beam simulated using the proposed semi-analytical model.

4.1.3 Case 3: Bi-Clamped Composite Plate-Like Beam with a Central Load

Finally, the model was validated using a concentrated mechanical load $F_0 = 1\ N$ in the z-direction, but now applied to a biclamped beam, as shown in Figure 4.5. The problem given by Equation 38 results in the equilibrium equation $[\boldsymbol{K}]\{\boldsymbol{q}\} = \{\boldsymbol{F_i}\}$, with concentrated load forces acting in the laminate as the vector $\{\boldsymbol{f_i}\} = \{0 \quad 0 \quad F_0\}^T$. The geometric boundary conditions

assured by Bardell functions combination were (Clamped-Free-Clamped-Free), using none of the first four polynomials in the ξ coordinate and all of the first four polynomials in the η coordinate.

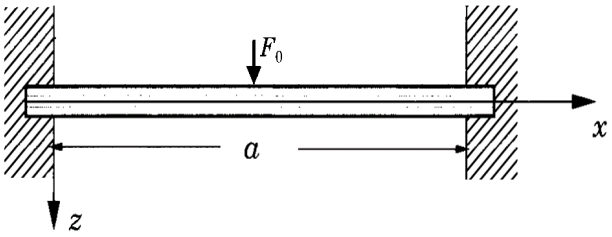

$$w_{mid-span} = \frac{F_0 a^3}{192EI}$$

FIGURE 4.5 – An example of biclamped beam with a mid-span mechanical load (Adapted from (REDDY, 2004)).

The typical deflection obtained through the closed-form solution is $w_{mid-span} = 1.0042\ mm$. The warpage and the maximum deflection (w_{max}) computed by simulation is shown in Figure 4.6. In this case, the proposed semi-analytical model also adopted 15 terms in the Bardell polynomial series for both the x and y directions.

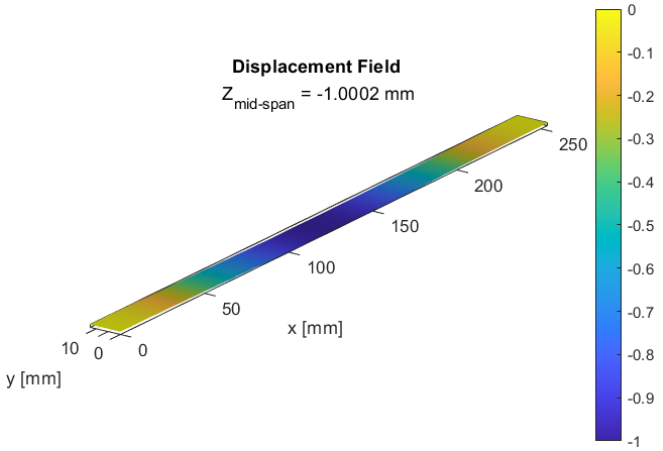

FIGURE 4.6 – The biclamped beam simulated using the proposed semi-analytical model.

All the results for maximum deflections, compared to those of the closed-form solution to the problem, are listed in Table 4.2 bellow. The convergence of the relative error is also presented by increasing the number of terms in the polynomial Bardell series.

TABLE 4.2 – Results for the symmetric composite beam simulated.

Beam problem type	**Number of terms Polynomial Series**	w_{max} **[mm] (proposed model)**	w_{max} **[mm] (Closed-Solution)**	**Relative error (%)**
cantilever beam loaded at tip	6	63.8476	64.2684	0.6548
	10	64.0903	64.2684	0.2772
	15	64.1566	64.2684	0.1740
cantilever beam with distributed load	6	23.9031	24.1007	0.8199
	10	24.0158	24.1007	0.3519
	15	24.0479	24.1007	0.2190
biclamped beam with punctured load	6	0.9275	1.0042	7.6316
	10	0.9928	1.0042	1.1296
	15	1.0002	1.0042	0.3945

The Figures 4.7 and 4.8 show the comparison between deflection distribution along length computed through the proposed semi-analytical model and the result obtained by the closed-form solution available by Megson (MEGSON, 2015). These comparisons are for a cantilever beam loaded at the tip and with a distribute load, respectively. The closed-form solution is given by deflection $w(x)$ computed in the neutral plane ($w(x)|_{y=0}$),

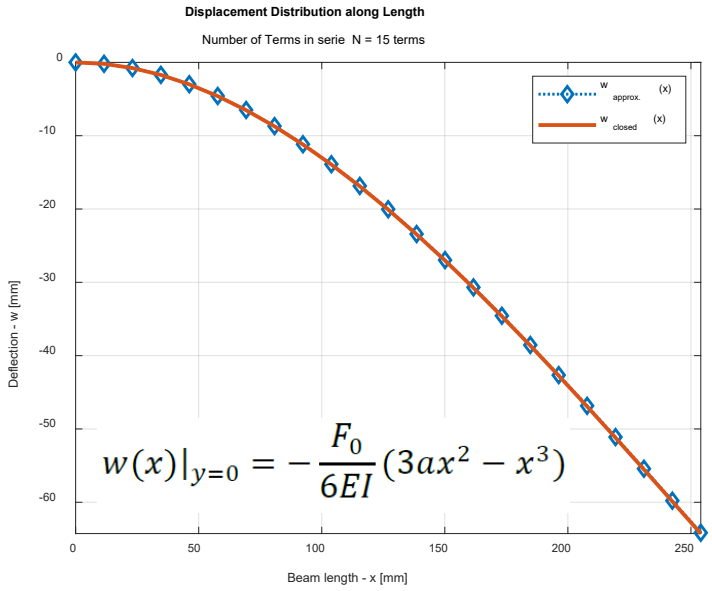

FIGURE 4.7 – Comparison of deflection along beam length, calculated from the proposed model and literature closed-solution for the clamped beam loaded at the tip.

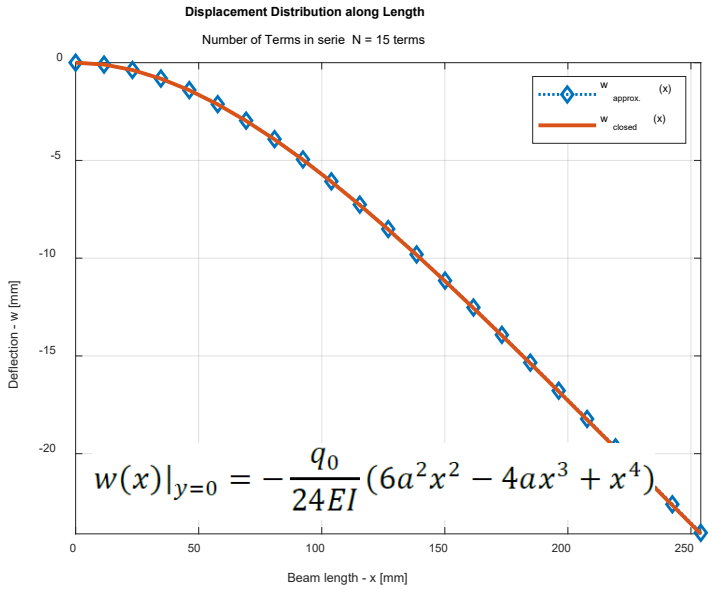

FIGURE 4.8 – Comparison of deflection along beam length, calculated from the proposed model and literature closed-solution for the clamped beam with distributed load.

After examining the previous Figures 4.7 and 4.8, along with the deflection values listed in Table 4.2 and their correspondent relative error results, it is possible verify that the proposed semi-analytical model is validated for the mechanical load. The Figures above show the good agreement for beam deflection along its length. All the geometric boundary condition of clamped at one edge and bi-clamped beam were simulated by selecting which of the first four polynomials should be considered in the function series, as mentioned in section 3.5.

4.2 Verification of the Proposed Semi-Analytical Model for Thermal Loading Cases

4.2.1 Case 1: Clamped-Free Bi-Material Plate-Like Beam Laminate Subjected to Thermal Loading

In order to validate the model for applied thermal loads, the analysis was carried out in a bi-material plate-like beam laminate composed by fabric layers of high-end thermoplastic composite material $[(0,90)/(+45,-45)]_{2S}$ with an aluminum layer at the bottom.

This stacking sequence using aluminum is a noncommercial layup intended to simulate a similar experiment carried out by Marques (MARQUES, 2023), which performed a comprehensive resin characterization and indirectly verified the warpage behavior in a bi-

material plate-like beam laminate due to thermal residual effects. The modelling of the experimental setup follows the content available in Cambridge website (THERMAL, 2022), as illustrated in Figure 4.9.

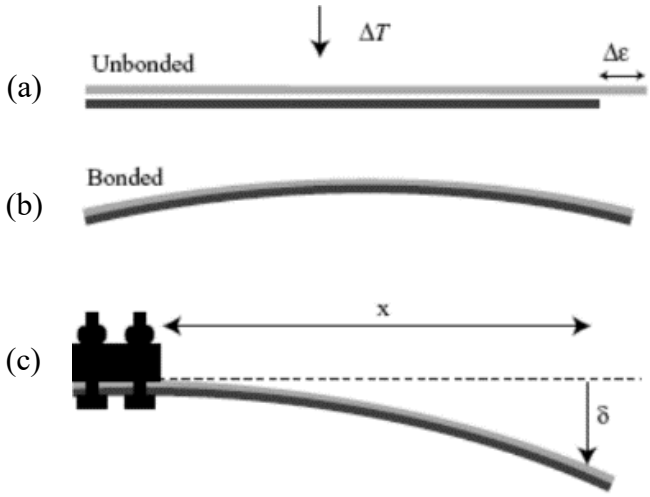

FIGURE 4.9 – An illustration of (a) bi-material beam experimental setup available in (THERMAL, 2022), (c) simulating a clamped bi-material plate-like beam laminate (bonded together) and (b) resulting internal stresses generating a uniform curvature when undergoes a temperature change ΔT.

According to the content in reference (THERMAL, 2022), the maximum deflection (δ) is function of the curvature (κ) of the bi-material beam, assuming that they are bonded and do not slip relative to each other. The exact solution is given in the Equation 40 below and can be calculated by the relaxation method or using available functions in commercial platforms to solve transcendental equations.

$$\kappa = \frac{2\sin\left[\tan^{-1}\left(\delta/_{x}\right)\right]}{\sqrt{(x^2+\delta^2)}} \tag{40}$$

The curvature is computed by an expression obtained from the moment balance, which arises from stress distribution due to misfit strains between the bonded materials. More detailed information can be found at (CLYNE, 1996). This curvature expression is given in Equation 41, and is related to constituents' material properties and their thickness,

$$\kappa = \frac{6(h_{Al} + h_C)h_{Al}h_C\Delta\varepsilon}{{E_{Al}}^2{h_{Al}}^4 + 4E_{Al}E_C{h_{Al}}^3h_C + 6E_{Al}E_C{h_{Al}}^2{h_C}^2 + 4E_{Al}E_C h_{Al}{h_C}^3 + {E_C}^2{h_C}^4} \tag{41}$$

Where h_{Al} and h_C are the thickness of aluminum and composite, respectively, the Elastic modulus are E_{Al} and E_C , and the misfit strain $\Delta\varepsilon$ is computed using the temperature step ΔT and the thermal expansion coefficients (α_{Al}, α_C) of constituents' materials, as given by Equation 42:

$$\Delta\varepsilon = (\alpha_{Al} - \alpha_C)\Delta T \tag{42}$$

The properties and engineering constants for both materials are given in Table 4.3. Each thermoplastic laminae have the same geometry values, $a = 200\,mm$, $b = 26\,mm$ and $t = 0.31\,mm$, while the aluminum layer has a thickness of $t = 1.25\,mm$.

TABLE 4.3 – Engineering properties of Toray Cetex® TC1225 High Strength T300JB 3K Carbon and aluminum layer of Al2024-T4

	$\boldsymbol{E_1}$ [MPa]	$\boldsymbol{E_2}$ [MPa]	$\boldsymbol{\upsilon_{12}}$	$\boldsymbol{G_{12}}$ [MPa]	$\boldsymbol{\alpha_1}$ [°C^{-1}]	$\boldsymbol{\alpha_2}$ [°C^{-1}]
TC1225	58	58	0.052	3.9	1.73x10^{-5}	1.73x10^{-5}
Aluminum	73.1	73.1	0.33	48.6	24.7x10^{-6}	24.7x10^{-6}

Using the proposed semi-analytical model, the problem given by Equation 38 results in the equilibrium equation $[\boldsymbol{K}]\{\boldsymbol{q}\} = \{\boldsymbol{F_f}\}$. The thermal load is derived from the simulated cure degree step for the resin, $\Delta T = T_{room} - T_{cure} = -115$ ℃, resulting in the midplane generalized thermal forces $\{\boldsymbol{f}\} = \{N_{xx}^T \quad N_{yy}^T \quad N_{xy}^T \quad M_{xx}^T \quad M_{yy}^T \quad M_{xy}^T\}^T$ applied to the laminate, computed following the Equation 14. The geometric boundary conditions assured by Bardell functions are the same as those given in Section 4.1.1 and 4.1.2.

The Figure 4.10 shows the warpage of the bi-material plate-like beam laminate using the semi-analytical model, considering only the thermal load applied to the cantilever plate-like beam configuration.

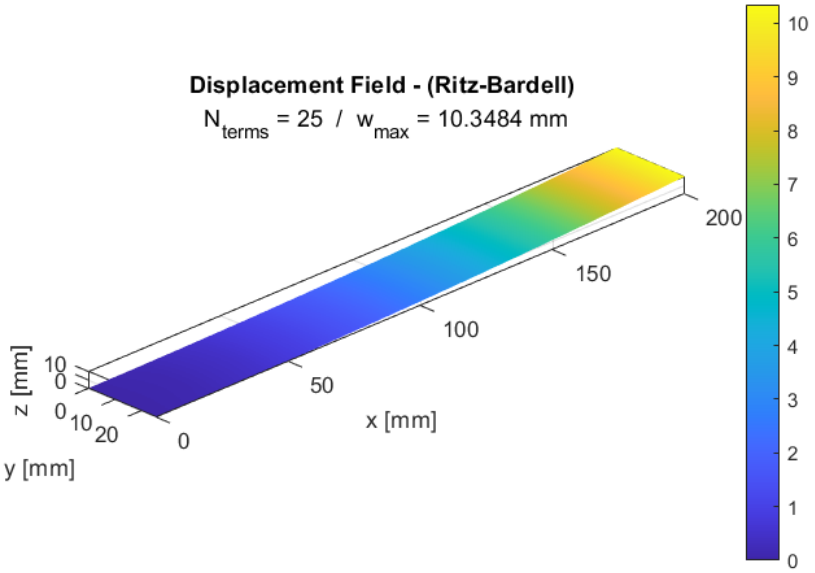

FIGURE 4.10 – The cantilever plate-like beam simulated using the present model.

The curvature and deflection relation given in Equation 40 was solved using the Matlab® "fzero" function, resulting in a maximum beam deflection of $\delta = 10.2405\ mm$. The results for deflections and convergence analysis with error achieved by the proposed semi-analytical model are listed in Table 4.4 below.

Table 4.4 – Results for cantilever bi-material plate-like beam laminate with thermal load only.

Number of terms Polynomial Series	w_{max} **[mm] (proposed model)**	w_{max} **[mm] (Closed-Solution)**	**Relative error (%)**
6x5	13.3678	10.2405	30.5385%
10x5	11.2003	10.2405	9.3725%
15x5	10.5974	10.2405	3.4551%
18x5	10.4683	10.2405	2.2245%
21x5	10.3986	10.2405	1.5438%
25x5	10.3844	10.2405	1.0536%

The convergence study evaluated up to 25 terms for the polynomial series in x direction while maintaining 5 terms in y direction. However, adding more than 18 additional terms resulted in a timeout of 1 hour during simulation. This issue arises from a code architecture where subcodes run sequentially, including one for derivation and integration of symbolic matrices, whose size is proportional to the number of terms in the polynomial series.

Thus, since the error between the exact solution and the simulated maximum deflection using 15 terms was approximately 3 %, and the magnitude of this difference was 0.35 mm, the

model convergence and accurate were considered satisfactory. Improved results and convergence rates could be achieved by enhancing the simulation code to run in parallel, and by changing the method to compute integration.

Since the results satisfactorily validated the developed model, demonstrating the possibility of achieving good results for thermal loads in bi-material laminates, the next step is to conduct simulations for laminate plates with specific geometric boundary conditions and subjected to the mechanical or thermal loads. These simulations will be compared with cases in the open literature or numerical results obtained by FEM.

4.2.2 Case 2: Monolithic Laminate Plate Subjected to Thermal Loading

In order to verify the approach with other geometries and materials, the model was applied to a non-symmetric [$90_2/0_2$] Carbon/Epoxy free plate under thermal load and compared to the CLT model. The engineering properties for material laminas with a thickness of $t = 0.19\ mm$ and dimensions $a = b = 200\ mm$ are listed in Table 4.5. The warpage of the plate according to the CLT model was calculated, resulting in the out-of-plane deflection ($w(x, y)$) given by Equation 43, available in chapter 8 of Daniel (DANIEL; ISHAI, 2006):

$$w(x, y) = -\frac{1}{2}\left(\kappa_x . x^2 + \kappa_y . y^2 + \kappa_{xy} . x . y\right) \tag{43}$$

TABLE 4.5 – Engineering properties of laminae constituents for (AS4/3501-6) (Adapted from (DANIEL; ISHAI, 2006)).

$\boldsymbol{E_1}$ [MPa]	$\boldsymbol{E_2}$ [MPa]	$\boldsymbol{\upsilon_{12}}$	$\boldsymbol{G_{12}}$ [MPa]	$\boldsymbol{\alpha_1}$ [°C^{-1}]	$\boldsymbol{\alpha_2}$ [°C^{-1}]
142000	10300	0.28	7200	-0.9x10^{-6}	27x10^{-6}

Figure 4.11a shows the warpage of the laminate and maximum displacements at z-direction calculate by Equation 43 for CLT model and using the curvatures obtained through the inversion of Equation 17, for the laminate under the thermal load only. The thermal load is derived from the simulated cure step for the resin, $\Delta T = T_{room} - T_{cure} = -115$ ℃, resulting in a generalized thermal forces and moments acting in midplane of the laminate $\{\boldsymbol{f}\} = \{N_{xx}^T \quad N_{yy}^T \quad N_{xy}^T \quad M_{xx}^T \quad M_{yy}^T \quad M_{xy}^T\}^T$.

The same load was used to compute the strains and curvatures using the proposed semi-analytical model. In this case, the problem given by Equation 38 results in the equilibrium equation $[\boldsymbol{K}]\{\boldsymbol{q}\} = \{\boldsymbol{F_f}\}$. The geometric boundary conditions assured by Bardell functions combination was (F-F-F-F), using all the four polynomials in the ξ and η coordinates. Figure 4.11b shows warpage of the laminate for the simulations with the proposed semi-analytical model, demonstrating the perfect match of maximum displacements at z-direction and the saddle shape when compared with the CLT results.

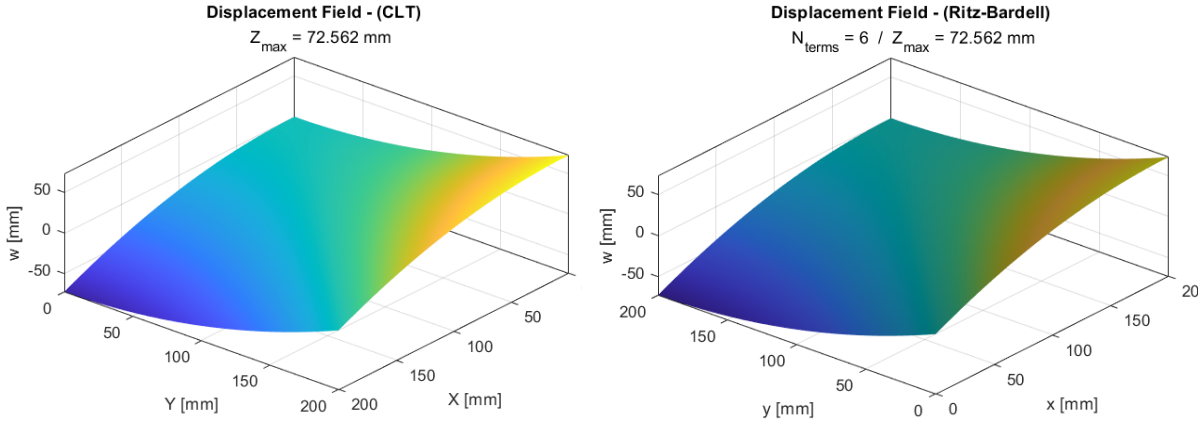

(a) (b)

FIGURE 4.11 – The warpage results using (a) CLT model for a non-symmetric $[90_2/0_2]$ composite free plate under thermal load and (b) through the proposed semi-analytical model.

The values of principal stresses in each layer are summarized in Table 4.7 below, indicating the residual stresses induced in the laminate by thermal load. Note that the sum of stresses in longitudinal direction results in the same value, but opposite in signal, compared to the sum of stresses in the transversal direction, thus canceling each other, as expected for a result of the non-symmetric layup under thermal load only.

TABLE 4.6 – Stresses distributed in each layer for $[90_2/0_2]$.

layer	σ_1 [MPa]	σ_2 [MPa]	τ_{12} [MPa]
1	-16.9313	16.9313	0
2	-113.3778	22.0727	0
3	-16.9313	16.9313	0
4	79.5152	11.7899	0
Σ	-67.7253	67.7253	0

To represent the tool-part interaction effect discussed in Chapter 2, a reinforcement layer of aluminum was added to the laminated composite plate. The aluminum layer has the same engineering constants listed in Table 4.3, and the same thickness of $t = 1.25\ mm$. The results for Semi-Analytical model are shown in Figure 4.12 below.

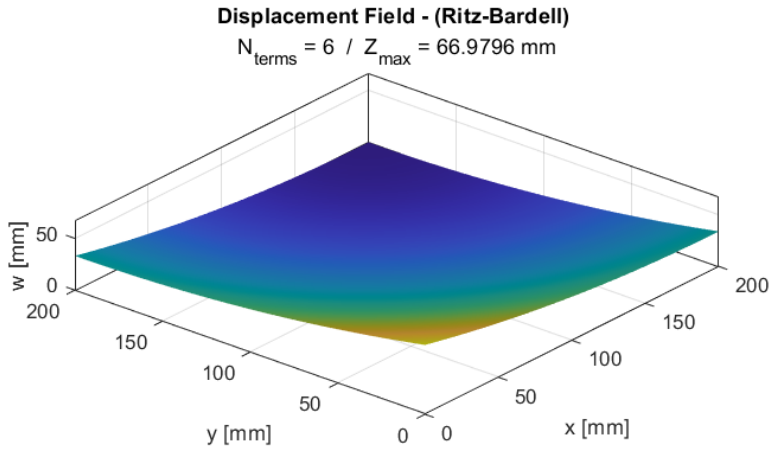

FIGURE 4.12 – Warpage result through simulation using the proposed semi-analytical model for a bi-material composite free plate [$90_2/0_2$/Al] under thermal load.

The results presented in Figures 4.11b and 4.12 intends to give an idea of the influence of the interaction between the tool-metal and a Carbon/Epoxy composite. The warpage in Figure 4.11b is greater than that in Figure 4.12. This behavior reflects the influence of the additional aluminum lamina in the second case, which prevents some of the warpage that occurs in the non-symmetric layup [$90_2/0_2$]. Thus, it can be inferred that the tool-part interaction contributes to the buildup of residual stresses in the composite upon tool removal.

4.2.3 Case 3: Cantilever Laminate Plate under Thermal Loading

Additionally, using a different layup configuration, the developed model was validated using a laminate with orthotropic stacking sequence [45/90/-75/-45] as found in Vermes (VERMES; CZIGANY, 2022), in which each lamina material is a Hexcel IM7/913 UD prepreg, and its properties are listed in Table 4.7 below. Each ply has a thickness of $t = 0.13\ mm$ and the dimensions are $a = b = 190\ mm$.

TABLE 4.7 – Engineering properties of laminae constituents for (Hexcel IM7/913 UD prepreg).

E_1 [MPa]	E_2 [MPa]	ν_{12}	G_{12} [MPa]	α_1 [°C^{-1}]	α_2 [°C^{-1}]
163300	8700	0.3	4500	3.0x10^{-7}	3.2x10^{-5}

The semi-analytical model developed was configured to simulate the composite plate with one edge fully restrained, i.e., Clamped-Free-Free-Free (C-F-F-F) configuration, as allowed by the combinations of Bardell functions. In his experimental work, Vermes (VERMES; CZIGANY, 2022) used a laminate that was treated in the autoclave at a plateau temperature of $140\ °C$, and cooldown to room temperature ($25\ °C$). This temperature profile was used in the present simulation.

The maximum deflection of the laminate plate occurred distant from the initial condition, and the result achieved by the proposed semi-analytical model around the corner was $w_{max} = 118.2138\ mm$, using 8 terms of the polynomial series in both directions, as shown in Figure 4.13a.

The obtained results were compared to numerical simulation in FEM using ABAQUS®, by adopting the following assumptions:

- The part was created in a 3D Modeling Space, deformable Type, using a Base Feature of Conventional Shell Planar Type (S4R) due to the thin characteristic of plate dimensions (thickness less than $t = 2\ mm$).
- Due to thinner plate characteristics, a quadratic function (second order elements) were chosen for the displacement of elements, to mitigate the numerical issue of overly stiff behavior known as shear locking effect. Additionally, enhanced hourglass control was applied to avoid the mesh instability when using reduced integration elements, ensuring proper shape distortions.
- A thermal load of $\Delta T = T_{room} - T_{cure} = -115$ ℃ was applied to define cooldown cure degree process.
- The resultant number of elements in the mesh was 9,025.

The result of simulation using FEM ABAQUS® showed a maximum deflection of approximately $w_{max} = 120.8400\ mm$, as shown in Figure 4.13b below. The Table 4.8 shows the results of both models employed.

(a)

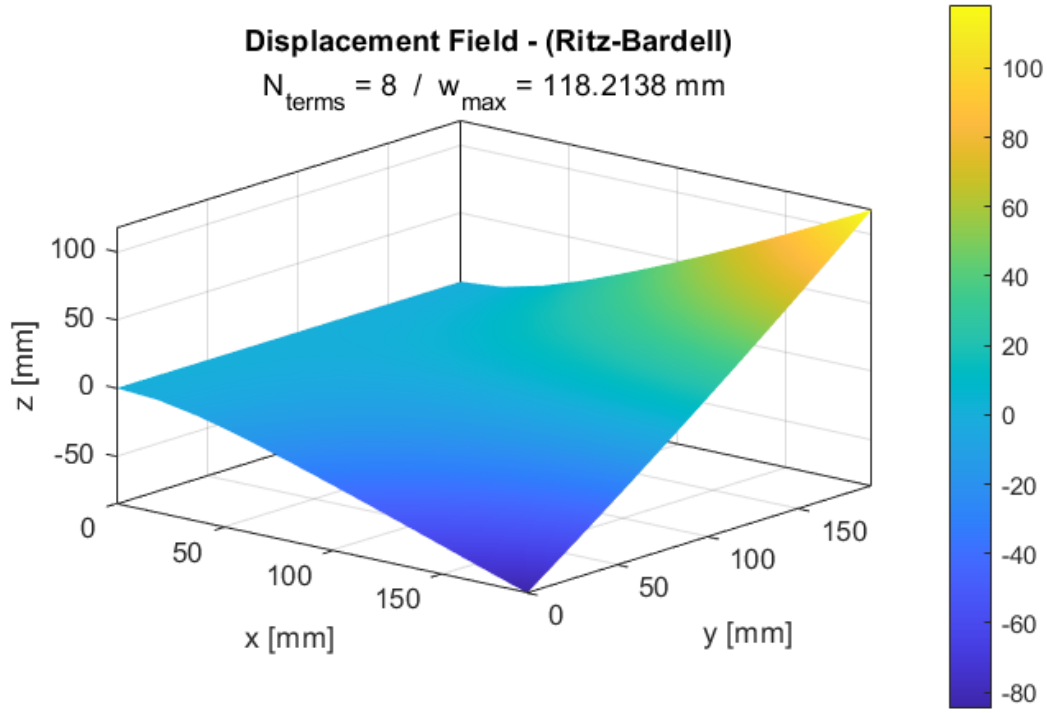

(b)

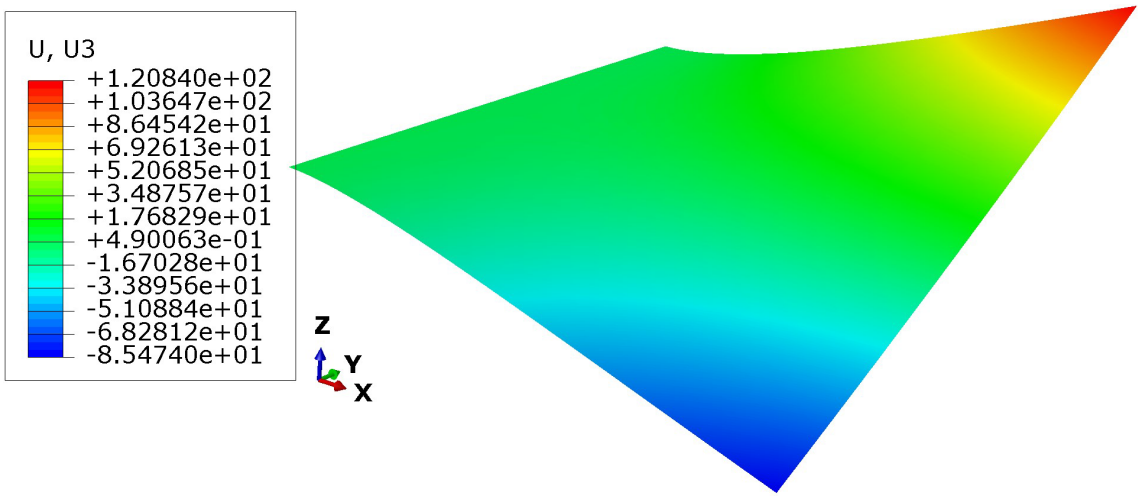

FIGURE 4.13 – Warpage result for the orthotropic laminate plate [45/90/-75/-45] clamped at one edge in y direction using (a) proposed semi-analytical model and (b) FEM ABAQUS®.

TABLE 4.8 – Comparison between results obtained from FEM and from the proposed Semi-Analytical model.

Method	**Number of terms Polynomial Series**	$w_{min-deflec}$ $[mm]$	**error**
FEM -ABAQUS	-	120.840	-
Semi-Analytical Model	6 x 6	115.355	4.5390 %
Semi-Analytical Model	7 x 7	117.0607	3.1275 %
Semi-Analytical Model	8 x 8	118.2138	2.1732 %

The same configuration of boundary conditions and thermal loads was applied to a composite orthotropic plate using numerical simulations at ABAQUS® and by the semi-analytical model proposed in this work (Rayleigh-Ritz using Bardell functions to describe the displacement-fields). Initially, 6 terms in the Bardell series were chosen for both directions, and the warpage result closely matched those obtained via FEM, as shown in Figures 4.13a and 4.13b, and in the maximum deflection values listed in Table 4.8. Once again, the thermal effects on laminate behavior during the curing process were demonstrated, highlighting the issues that arise in the fabrication process. This simulation also included a boundary restriction commonly encountered in the fabrication of laminate plates and panels.

5 Conclusion

The simulations performed using the proposed semi-analytical model yield results that agree fairly well with those obtained through closed-form solutions, exact solutions, and the finite element (FE) method, for both mechanical and thermal loads. The model was validated under various conditions, including different materials such as thermosetting polymers like E-Glass/Epoxy and Carbon Fiber/Epoxy (AS4/3501-6), thermoplastic materials (Toray Cetex® TC1225 High Strength T300JB 3k Carbon), unidirectional lamina (Hexcel IM7/913 UD prepreg), and a bi-material composite plate with an Aluminum layer (Al2024-T4).

The model's predictions were compared against exact solutions and finite element simulations for different loading and boundary conditions, showing excellent correlation. This includes validation for a laminate beam under mechanical load and thermal load applied to a bi-material plate-like beam laminate, as demonstrated in Section 4.2.

In certain cases, a convergence study was performed, indicating the necessity of addition of higher order to enhance result accuracy. This need is demonstrated by the error results presented in Section 4.1.3, which analyzes a biclamped beam under mechanical load (see Figure 4.6), and in Section 4.2.1, which examines a bi-material plate-like beam laminate under thermal load (see Figure 4.10).

The convergence study revealed that specific cases may require an increase in the number of terms of polynomial series. This highlights some limitations of the current model and suggests the need for considering approximation functions with improved convergence properties.

In the analysis performed on the bi-material plate-like beam laminate, as demonstrated in Section 4.2, the warpage results highlighted a significant aspect of thermal effects on laminates. These findings underscore the importance of considering thermal effects in composite fabrication and operation, as their influence cannot be overlooked. The results presented indicate that for bi-material non-symmetric laminates, the influence of reinforcement layers, such as aluminum, plays a crucial role in warpage outcomes. This underscores the necessity of considering any reinforcement layer during the composite laminate design process to achieve the desired geometry of the final part.

Additionally, the interaction between the composite laminate and the mold during the curing process significantly impacts the final geometry of the part. This Tool-Part Interaction

is clearly demonstrated by the results in Section 4.2.2 for monolithic plates. For a bi-material laminate layup, the warpage behavior is attenuated due to the interaction between the composite and aluminum material. As shown in Figure 4.12, the bi-material laminate shows reduced warpage compared to conventional composite laminates, as illustrated in Figure 4.11, which exhibits significant warping due to the nonsymmetric layup.

Furthermore, the warpage behavior in composite plates due to thermal effects is significantly influenced by mold constraints, as demonstrated in the last simulation of an orthotropic laminate plate with a clamped edge (refer to Figure 4.13). These effects can be effectively captured by the proposed semi-analytical model, as evidenced by the close agreement with the results from numerical simulations using FEM.

According to the objectives of this work, the developed computational tool provides valuable insights for the design and manufacturing process, allowing to prevent geometric distortions and residual stresses in laminates.

The model proposed herein is suitable for the exploratory application of the Rayleigh-Ritz approximation solution using Bardell polynomial functions, which is the main contribution of this work. Therefore, it is possible to conclude that the proposed approach calculates the residual strains and stresses during the cure cycle of laminate fabrication, emphasizing the substantial impact of residual thermal loads on the final geometry of the part.

5.1 Future Works

Future work includes extending the proposed formulation to address the kinetics of cure involved in laminate fabrication. This extension would enable the prediction of significant effects such as chemical and hygroscopic residual stresses. This can be accomplished by using the viscoelastic behavior of composite constituents, such as shrinkage coefficients, or by employing phenomenological models, including time-dependent or path-dependent models, where changes in the engineering properties of fiber and matrix can be tracked.

The current model could be compared with thick plate theory analyses available in the literature to potentially enhance the model by including transverse shear stresses.

Moreover, the present model can be extended by changing the strain-displacement field from a linear to a nonlinear relationship, such as Von-Kármán relations, to handle more complex geometries such as shells and cylinders.

In a more detailed investigation, resin characterization could be conducted to convey more accuracy to the model. Experimental setups for plates or clamped beams could validate the model against real-world data, providing further confidence in its predictive capabilities.

By addressing these areas, the robustness and applicability of the semi-analytical model can be significantly enhanced, providing a more comprehensive tool for analyzing thermo-mechanical stresses in composite laminates.

Bibliography

ABOUHAMZEH, M.; SINKE, J.; BENEDICTUS, R. Prediction models for distortions and residual stresses in thermoset polymer laminates: an overview. **Journal of Manufacturing and Materials Processing**, v. 3, n. 4, p. 87, 2019.

ALLEN, D. H.; HAISLER, W. E. **Introduction to aerospace structural analysis**. Texas: John Wiley and Sons, 1985. 507p. ISBN 0-471-88839-7.

CLYNE, T. W. Residual stresses in surface coatings and their effects on interfacial debonding, **key Engineering Materials**, v. 116-117, p. 307-330, 1996.

BARDELL, N. S. Free vibration analysis of a flat plate using the hierarchical finite element method. **Journal of Sound and Vibration**, v. 151, n. 2, p. 263-289, 1991.

CHEN W.; ZHANG D. A micromechanics-based processing model for predicting residual stress in fiber-reinforced polymer matrix composites. **Composite Structures**, v. 204, p.153–16, 2018.

DANIEL, I. M.; ISHAI, O. **Engineering mechanics of composites**. 2. ed. New York: Orford University Press, 2006, 463 p. ISBN 978-0-19-515097-1.

FERNLUND, G.; OSOOLY, A.; POURSARTIP, A.; VAZIRI, R.; COURDJI, R.; NELSON, K.; GEORGE, P.; HENDRICKSON, L.; GRIFFITH, J. Finite element-based prediction of process-induced deformation of autoclaved composite structures using 2D process analysis and 3D structural analysis. **Compos. Struct.,** v. 62, n. 2, p. 223–234, 2003. ISSN 02638223.

GONZÁLEZ-CANTERO, J. M.; GRACIANI, E.; BLÁZQUEZ, A.; PARÍS, F. A new analytical model for evaluating interlaminar stresses in the unfolding failure of composite laminates. **Composite Structures**, v. 147, p. 260–273, 2016.

JONES, R. M. **Mechanical of composite materials**. 2. ed. New York: Taylor Francis, 1999. 538p. ISBN 1-56032-712-X.

REDDY, J. N. **Introduction to the finite element method**. 4. ed. Texas: McGraw Hill Education, 2019. 1151p. ISBN 978-1-25-986190-1.

REDDY, J. N. Mechanics of laminated composite plates and shell theory and analysis. 2. ed. Boca Raton: CRC Press, 2004. 858p. ISBN 0-8493-1592-1.

KAPPEL, E.; STEFANIAK, D.; FERNLUND, G. Predicting process-induced distortions in composite manufacturing: a pheno-numerical simulation strategy, **Compos. Struct.,** v. 120, p. 98–106, 2015. ISSN 02638223.

LAWRENCE, E. N. Cross-linking–effect on physical properties of polymers, **Journal of Macromolecular Science, Part C**: Polymer Reviews, v. 3, n. 1, p. 69-103, 1969.

LIMA, A. S.; FARIA, A. R.; FARIA, J. J. R. Critical review of displacement-based laminate theories and modelling techniques. *In*: BRAZILIAN CONFERENCE ON COMPOSITE MATERIALS, 4., 2018, Rio de Janeiro. **Proceedings** […]. Rio: BCCM, 2018. p. 10-17. https://doi.org/doi/10.21452/bccm4.2018.01.02.

LUCENA NETO, E. **Fundamentos da mecânica das estruturas**. Florianópolis: Orsa Maggiore, 2021. 523p. ISBN 978-65-993681-2-7

MAGDALENA U. A relationship between the glass transition temperature and the conversion degree in the curing reaction of the EPY® epoxy system. **Polimery**, v. 56, n. 3, p. 240-243, 2011.

MAKINDE, O. M. **Prediction of shape distortions in composite structures**. 2018. 207f. Thesis (Doctor of Science) – Instituto Tecnológico de Aeronáutica, São José dos Campos, 2018.

MARQUES, S. S. L. **Thermal Analysis of PA6 and residual strain characterization in PA6/woven carbon thermoplastic composite**. 2023. 96f. Dissertation (Master of Science) – Instituto Tecnológico de Aeronáutica, São José dos Campos, 2023.

MEGSON, T. H. G. **Aircraft structures for engineering students**. 4. ed. Burlington: Elsevier, 2015. 824p. ISBN-10 978-0-75066-7395.

NIELSEN, M. W. **Prediction of process induced shape distortions and residual stresses in large fibre reinforced composite laminates:** with application to wind turbine blades. 2012. Thesis (PhD) - Technical University of Denmark, Lyngby, 2012.

SINKE, J.; WANG, Y.; ABOUHAMZEH, M.; BENEDICTUS, R. Process induced warpage in laminated shells. *In*: INTERNATIONAL CONFERENCE ON COMPOSITE MATERIALS, 19., 2013, Toronto. **Proceedings** […]. Toronto: ICCM, 2013. p. 2575 – 2582.

SVANBERG, J. M.; HOLMBERG, J. A.; Prediction of shape distortions Part I. FE-implementation of a path dependent constitutive model. **Composites:** Part A Appl. Sci. Manuf., v. 35, n. 6, p. 711–721, 2004. ISSN 1359835X.

SVANBERG, J. M.; HOLMBERG, J.A. Prediction of shape distortions. Part II. Experimental validation and analysis of boundary conditions. **Composites:** Part A. Appl. Sci. Manuf**.**, v. 35, n. 6, p. 723–734, 2004. ISSN 1359835X.

SVANBERG, J. M.; ALTKVIST, C.; NYMAN, T.; Prediction of Shape Distortions for a Curved Composite C-spar. **Journal of Reinforced Plastics and Composites,** v. 24 n. 3, p. 323-339, 2005. DOI: 10.1177/0731684405043559.

THERMAL Expansion and the Bi-Material Strip (all content). Cambridge: University of Cambridge, 2022. Available at: https://www.doitpoms.ac.uk/tlplib/thermal-expansion/printall.php. Accessed on: 16th April 2024.

VERMES, B.; CZIGANY, T. Thermally induced mechanical work and warpage compensation of asymmetric laminates. **Composite Structures,** v. 295, 115847, 2022.

WISNOM, M. R.; GIGLIOTTI, M.; ERSOY, N.; CAMPBELL, M.; POTTER, K. D. Mechanism generating residual stresses and distortion during manufacture of polymer–matrix composite structures. **Composites:** Part A Appl. Sci. Manuf., v. 37, n. 4, p.522-529, 2006. ISSN 1359835X.

YUAN, Z.; WANG, Y.; PENG, X.; WANG, J.; WEI S. An analytical model on through-thickness stresses and warpage of composite laminates due to tool-part interaction, **Composites Part B,** v. 91, p.408-413, 2016.

Appendix A – Micromechanics and Glass Transition

A.1 Engineering Properties of Lamina Changing During Cure

This Appendix shows the equations adopted in the micromechanics model, in order to represent the engineering properties changes of a laminae during the cure cycle, when a phase transformation from liquid to glassy state occurs with the resin. This transformation is assumed to follow the DiBenedetto equation (LAWRENCE, 1969), to represent the cure degree update.

$$\frac{T_g - T_{g_0}}{T_{g_\infty} - T_{g_0}} = \frac{\lambda\chi}{(1-(1-\lambda)\chi)} \qquad (A.1)$$

Where χ is the degree of cure of the resin, λ is a structure-dependent parameter with a value between 0 and 1, T_{g_0} is the glass transition temperature of the uncured resin (when $\lambda = 0$), and T_{g_∞} is the glass transition temperature of the fully reacted resin ($\lambda = 1$), (MAGDALENA, 2011).

Equation A.1 presents the relationship between the glass transition temperature (T_g) and χ, which determines when vitrification occurs during curing of the resin. This characteristic strongly affects the elastic properties of resin, such as Young and Shear Modulus, Poisson´s coefficient, as well as the CTE, which assumes different values for each phase change.

To elucidate, Table A.1 presents the values of these parameters for Araldite LY5052/Hardener HY5052 extracted from Svanberg (SVANBERG; HOLMBERG, 2004b), and Carbon Fabric Hexcel AGP193-P extracted from Daniel (DANIEL; ISHAI, 2006).

TABEL A.1 - Resin and fiber physical Properties of LY5052 epoxy matrix and Hexcel AGP193-P.

Resin rubbery state		**Resin glassy state**		**Fiber**	
$\boldsymbol{E_m^{rub}}$	28 MPa	E_m^{gly}	2600 MPa	E_f	235000 MPa
$\boldsymbol{\upsilon_m^{rub}}$	0.497	υ_m^{gly}	0.38	υ_f	0.2
$\boldsymbol{G_m^{rub}}$	9.4 MPa	G_m^{gly}	940 MPa	G_f	27000 MPa
$\boldsymbol{\alpha_m^{rub}}$	178x10^{-6} °C^{-1}	α_m^{gly}	71x10^{-6} °C^{-1}	α_f	-0.5x10^{-6} °C^{-1}
$\boldsymbol{\beta_m^{rub}}$	-2.33 %	β_m^{gly}	-2.33 %	β_f	0

Such changing of resin parameters during different phases, such as rubbery and glassy state, directly affects the lamina composite parameters. Consequently, the engineering properties of the lamina, such as Longitudinal, Transverse and Shear Modulus, as well Poisson´s coefficient, will undergo changes in their values during cure schedule. Additionally, this temperature changing will influence the CTE and Chemical Shrinkage Coefficient in the longitudinal and transversal directions for a Carbon-Epoxy laminae over time, following the micromechanical behavior and fiber and matrix mixture rule (DANIEL; ISHAI, 2006), as described by Equations A.1 to A.9.

$$E_1 = E_m(T,\chi)V_m + E_f V_f \tag{A.2}$$

$$\frac{1}{E_2} = \frac{V_m}{E_m(T,\chi)} + \frac{V_f}{E_f} \tag{A.3}$$

$$\upsilon_{12} = V_m \upsilon_m(T,\chi) + V_f \upsilon_f \tag{A.4}$$

$$\frac{1}{G_{12}} = \frac{V_m}{v(T,\chi)} + \frac{V_f}{G_f} \tag{A.5}$$

$$\alpha_1 = \frac{1}{E_2}\left(\alpha_f E_f V_f + \alpha_m(T,\chi)E_m(T,\chi)V_m\right) \tag{A.6}$$

$$\alpha_2 = \left(1+\upsilon_f\right)\alpha_f V_f + \left(1+\upsilon_m(T,\chi)\right)\alpha_m(T,\chi)V_m - \alpha_1\upsilon_{12} \tag{A.7}$$

$$\beta_1 = \frac{1}{E_1}\left(\beta_f E_f V_f + \beta_m(T,\chi)E_m(T,\chi)V_m\right) \tag{A.8}$$

$$\beta_2 = \left(1+\upsilon_f\right)\beta_f V_f + \left(1+\upsilon_m(T,\chi)\right)\beta_m(T,\chi)V_m - \beta_1\upsilon_{12} \tag{A.9}$$

Where V_f and V_m represent the volume fractions of each constituent (fiber and matrix), and the values of $E_m(T,\chi)$, $G_m(T,\chi)$, $\upsilon_m(T,\chi)$, $\alpha_m(T,\chi)$, and $\beta_m(T,\chi)$ are taken from Table A.1, depending on whether the resin is under rubbery or glassy state. The equations that represent this update of constituents' parameters related to degree of cure and temperature are shown in Equations A.10 to A.16 below.

$$E_m(T,\chi) = \begin{cases} 0, & if\ \ \chi < \chi_g, \qquad T \geq T_g(\chi) \\ E_m^{rub}, & if\ \ \chi \geq \chi_g, \qquad T \geq T_g(\chi) \\ E_m^{gly}, & if\ T < T_g(\chi) \end{cases} \tag{A.10}$$

$$\upsilon_m(T,\chi) = \begin{cases} 0, & if\ \ \chi < \chi_g, \qquad T \geq T_g(\chi) \\ \upsilon_m^{rub}, & if\ \ \chi \geq \chi_g, \qquad T \geq T_g(\chi) \\ \upsilon_m^{gly}, & if\ T < T_g(\chi) \end{cases} \tag{A.11}$$

$$G_m(T,\chi) = \begin{cases} 0, \quad if \ \ \chi < \chi_g, \qquad T \geq T_g(\chi) \\ G_m^{rub}, \quad if \ \ \chi \geq \chi_g, \qquad T \geq T_g(\chi) \\ G_m^{gly}, \quad if \ T < T_g(\chi) \end{cases} \tag{A.12}$$

$$\alpha_m(T,\chi) = \begin{cases} 0, \quad if \ \ \chi < \chi_g, \qquad T \geq T_g(\chi) \\ \alpha_m^{rub}, \quad if \ \ \chi \geq \chi_g, \qquad T \geq T_g(\chi) \\ \alpha_m^{gly}, \quad if \ T < T_g(\chi) \end{cases} \tag{A.13}$$

$$\beta_m(T,\chi) = \begin{cases} 0, \quad if \ \ \chi < \chi_g, \qquad T \geq T_g(\chi) \\ \beta_m^{rub}, \quad if \ \ \chi \geq \chi_g, \qquad T \geq T_g(\chi) \\ \beta_m^{gly}, \quad if \ T < T_g(\chi) \end{cases} \tag{A.14}$$

Table A.2 shows the resultant engineering properties for a Carbon/Epoxy lamina, obtained from micromechanics relations previously presented. These properties are based on the resin and fiber properties listed in Table A.1, with a composition of 60% and 40%, respectively.

TABLE A.2 – Resultant Engineering properties of a Carbon/Epoxy lamina.

E_1 [MPa]	E_2 [MPa]	υ_{12}	G_{12} [MPa]	α_1 [°C^{-1}]	α_2 [°C^{-1}]
142040	6394	0.272	2233	2.35x10^{-8}	3.88x10^{-5}

The effects of time changing in the lamina properties, CTE and Chemical Shrinkage Coefficient, during a hypothetical cure cycle, are illustrated in Figures 2.2 and 2.3 using Equations A.1 to A.14. The assumptions include temperature rate and cure degree rate given by Equations A.15 and A.16, respectively:

$$T_{rate} = \frac{T_{room} - T_{cure}}{t_{final} - t_{cure}} \tag{A.15}$$

$$\chi_{rate} = \frac{1}{t_{cure}} \tag{A.16}$$

where T_{cure} is the temperature at polymer of matrix starts the liquid-rubbery transition at instant t_{cure} during the curing process, and T_{room} is the room temperature reached by the composite at the end of the curing process, at instant t_{final} . The hypothetical values for these variables were $T_{cure} = 140$℃ and $T_{room} = 25$℃, for a time process of $t_{final} = 20h$, with curing starts at instant $t_{cure} = 12h$.

FOLHA DE REGISTRO DO DOCUMENTO

1. CLASSIFICAÇÃO/TIPO	2. DATA	3. REGISTRO N	4. N DE PÁGINAS
DM	23 de julho de 2024	DCTA/ITA/DM-055/2024	75

5. TÍTULO E SUBTÍTULO:

A Semi-Analytical Model for Thermo-Mechanical Stress Analysis in Composite Laminates

6. AUTOR(ES):

Danilo Moura Prata

7. INSTITUIÇÃO(ÕES)/ÓRGÃO(S) INTERNO(S)/DIVISÃO(ÕES):

Instituto Tecnológico de Aeronáutica – ITA

8. PALAVRAS-CHAVE SUGERIDAS PELO AUTOR:

1.Rayleigh-Ritz 2. Bardell functions 3. Thin Plate Theory 4. Thermal residual stresses 5. Composite laminate

9.PALAVRAS-CHAVE RESULTANTES DE INDEXAÇÃO:

1. Materiais compósitos 2. Deformação 3. Método de Rayleigh-Ritz 4. Laminados 5. Tensão residual 6. Engenharia de materiais

10. APRESENTAÇÃO: **(X) Nacional ( ) Internacional**

ITA, São José dos Campos. Curso de Mestrado. Programa de Pós-Graduação em Engenharia Aeronáutica e Mecânica. Área de Projeto Aeronáutico, Estruturas e Sistemas Aeroespaciais. Orientador: Prof. Dr. Maurício Vicente Donadon. Defesa em 21/06/2024. Publicada em 2024.

11. RESUMO:

Composite materials made up of high modulus carbon fiber and thermoset resin have been used in advanced engineering structures across a range of sectors, such as oil exploration, aerospace, wind energy, among others. However, undesired small deformations occurs during the manufacturing of these materials, in the curing process responsible for perfect adhesion between the fiber and matrix constituents. These deformations result in residual stresses that can lead to geometric distortions in the final part or reduce the material's strength, a characteristic highly valued by designers when adopting composite materials. These residuals stresses originate from effects of different natures, such as thermal, chemical and even hygroscopic, which occur in the composite constituents due to thermal gradients and material characteristics under the conditions of humidity and pressure, interaction of the part with the mold, characteristics of each manufacturing process. The analysis and calculation of these stresses can be found in specialized literature; however, several authors, have developed adapted methodologies to calculate and predict deformations and stresses. The purpose of this study was to develop and implement a computational tool to simulate the effects of thermal residual deformations and stresses. The adopted approach is based on the Principle of Stationary of the Total Potential Energy of the system, allowing the analysis of linear or non-linear systems, considering the internal deformation energy and the potential of the forces applied to the system. The solution to the equilibrium of the system is to minimize the total potential energy, using the Rayleigh-Ritz approximation method to determine the generalized coefficients of the series of functions in the equilibrium equations, using Bardell functions to describe strain-displacement relations. The validation of the methodology is demonstrated through comparison with cases where closed solutions exist for mechanical loading problems, the exact solution for a thermal loading problem, and finite element simulations using the ABAQUS® commercial software, demonstrating the effectiveness of the adopted approach.

12. GRAU DE SIGILO:

(X) OSTENSIVO **( ) RESERVADO** **( ) SECRETO**